Synthetic ability of dinuclear mesocates containing 1,3-bis(diazinecarboxamide)benzene bridging ligands to form complexes of increased nuclearity. Crystal structures, magnetic properties and theoretical studies

Synthetic ability of dinuclear mesocates containing 1,3-bis(diazinecarboxamide)benzene bridging ligands to form complexes of increased nuclearity. Crystal structures, magnetic properties and theoretical studies.

*Maria A. Palacios,[a] Jessica Morlieras,[a] Juan Manuel Herrera,[a] * Antonio J. Mota,[a] Euan K. Brechin,[b] Smail Triki[c] and Enrique Colacio[a,*]*

[a] *Departamento de Química Inorgánica, Universidad de Granada, Av. Fuentenueva S/N, 18071 Granada (Spain)*

[b] *School of Chemistry. The University of Edinburgh, David Brewster Road, Edinburgh, EH9 3FJ (United Kingdom).*

[c] *UMR CNRS 6521, Université de Bretagne Occidentale, BP 809, 29285 Brest Cedex, (France)*

Abstract

Triple stranded Ni^{II}_2-metallacyclic complexes $Na_{2.5}[Ni_2(bpcb)_3]\cdot 0.5OH\cdot 18.5H_2O$ (**1**) and $Na_2[Ni_2(bpzcb)_3]\cdot 16H_2O$ (**2**), and double stranded Cu^{II}_2-metallacyclic complexes $[Cu_2(bpcb)_2(H_2O)_2]\cdot 3H_2O$ (**3**) and $[Cu_2(bpzcb)_2(H_2O)_2]\cdot 2H_2O$ (**4**) have been assembled from the tailored bisbidentate bridging ligands, 1,3-bis(pyrimidine-2-carboxamide)benzene (H_2bpcb) and 1,3-bis(pyrazine-2-carboxamide)benzene (H_2bpzcb), and the corresponding nitrate salts of the metal ions. Following the "complex as ligand" strategy, **1** can be assembled with either Ni^{2+}, Co^{2+} ions or the [Mn(acen)Cl] complex to afford unique, neutral, bent trinuclear molecules $[M^{II}Ni^{II}_2(bpcb)_3]\cdot x H_2O$ (**5** and **6**) and the 2D honeycomb-like complex $(PPh_4)\{[Ni_2(bpcb)_3]_2[Mn(acen)]_3\}$ (**7**), respectively. In these cases, the Ni_2 units are linked to the corresponding metal ions through amidate oxygen atoms and the outward nitrogen atom of one of the pyrimidine rings of the bcpb ligand. The assembly of **2** with Ln^{3+} ions (Ln^{3+} = Tb, Gd) leads to one dimensional complexes of formulae $[\{[Ni_2(bpzcb)_3]Tb(H_2O)_5\}(CF_3SO_3)\cdot THF\cdot 5H_2O]_n$ (**8**) and $[\{[Ni_2(bpzcb)_3]Ln(H_2O)_4(NO_3)\}\cdot 2THF\cdot nH_2O]_n$ (**9** and **10**) (Ln^{3+} = Gd and Tb), where the dinuclear Ni_2 units are joined to two Ln^{3+} ions exclusively through amidate oxygen atoms of two different ligands. The analyses of the magnetic data indicate that **1**-**4** exhibit intradinuclear ferromagnetic interactions between the metal ions through a spin polarisation mechanism, as supported by DFT calculations. Trinuclear complexes **5** and **6** show predominant antiferromagnetic coupling, which is a result of an antiferromagnetic interaction between one of the Ni^{2+} ions of the Ni_2 unit and the M^{2+} ion through the pyrimidine bridging fragment that is stronger

than the polarised ferromagnetic interaction between the Ni^{2+} ions through the bpcb ligand in the dinuclear $[Ni_2(bpcb)_3]^{2-}$ moiety. Complex **7** shows a dominant antiferromagnetic interaction between the Ni^{2+} and Mn^{2+}, whereas the Ni_2Ln (Ln^{3+} = Gd, Tb) chain complexes present ferromagnetic interactions inside the Ni_2 mesocate unit as well as between the Ni^{2+} ions of the Ni_2 unit and the Ln^{3+} ions. The magnetic exchange interactions in these new materials have been experimentally analysed and supported by theoretical DFT studies.

Introduction

In the last few decades, metallacycle complexes have been extensively used not only as models for the auto-assembly of supramolecular structures through metal ions, but also because of their involvement in new areas of research such as anion sensors, bioinorganic chemistry, luminescence, magnetism and molecular spintronics.[1-4] Among them, those prepared from aromatic dicarboxamide[2,3] or diimine[4] disubstituted benzene (or pyridine) ligands present magnetic coupling between metal ions through a spin polarisation mechanism. The nature of the magnetic interactions depends on the position of the substituents on the benzene ring. It has been proven from theoretical and experimental studies that 1,3-disubstituted benzene ligands give rise to ferromagnetic interactions (F), whereas 1,4-disubstituted benzene ligands generate antiferromagnetic interactions (AF). Therefore, the sign of the magnetic interactions depends on the number of aromatic atoms located in between the coupled magnetic ions. Indeed, odd numbers of atoms (using, for instance, *m*-phenylene linkers) lead to F interactions, whereas even numbers of atoms (using, for instance, *p*-phenylene linkers) lead to AF interactions. This is because the π-conjugated moiety exhibits an alternation of spin sign along the exchange pathway. In view of the above considerations, the design of the ligand, with specific functional groups, coordination modes and distance between the coordination sites, is a crucial factor for controlling the nature and magnitude of the magnetic coupling between the paramagnetic metal ions.

A number of pro-metallacycle ligands have been designed thus far which have been able to afford metallacycles with magnetic coupling between metal ions through a spin polarisation mechanism.[1h-j,2,3,4] One of the first reported examples was the ligand *N,N'-1,3-phenylenebis(oxamate)* (mpba), which in a self-assembly process with Cu^{2+} ions led to double stranded dinuclear complex showing strong ferromagnetic coupling between the metal ions due to spin polarisation of the electronic cloud of the *m*-substituted aromatic ring (Scheme 1).[5] Dinuclear mesocate metallacyles were also prepared with this kind of ligand and other metal ions (Ni^{2+}, Co^{2+}), which showed the expected magnetic coupling through a spin polarisation mechanism.[1i,3] Further, these dinuclear helicates were used to obtain structures with larger nuclearity through the non-coordinated donor atoms of the ligands, using the well-known "complex as ligand" strategy.[1i,2,3] Experimental results, as well as theoretical studies on dinuclear copper(II) complexes with bisbidentate bridging ligands containing *m*-phenylene linkers, have shown that the magnitude of the ferromagnetic interaction between the metal ions can be tuned by the electronic effects of the groups joined to the *m*-

phenylene moiety.[3,4] Indeed, groups that increase the spin density on the *m*-phenylene region can lead to enhanced ferromagnetic exchange interactions and *vice-versa*.

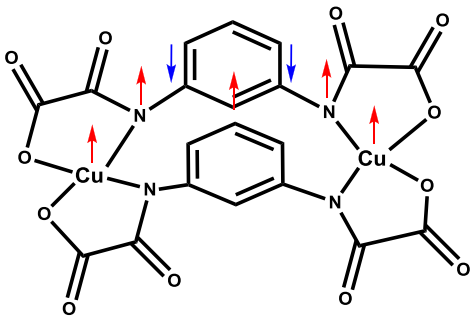

Scheme 1: Structure of dinuclear Cu metallacycle using the ligand N,N'-1,3-phenylenebis(oxamate)

In this context, our group designed a bisbidentate dinucleating bridging ligand, H_2mbpb (*1,3-bis(pyridine-2-carboxamide)benzene*) containing a *m*-phenylene linker with the aim of obtaining dinuclear complexes with comparatively stronger ferromagnetic interactions.[3] Thus, a series of double and triple stranded dinuclear metal complexes of formula $[Cu_2(mbpb)_2]\cdot 2H_2O$, $[Ni_2(Hmbpb)_3](PF_6)\cdot 21H_2O$ were prepared and their magnetic properties studied.[3] These complexes exhibited, as expected, ferromagnetic coupling between the metal ions by spin polarisation through the bridging ligand. It is worth noting that the Cu^{2+} derivate exhibited the strongest magnetic exchange interaction (J = +21.1 cm^{-1}) so far reported for Cu^{2+} dinuclear complexes containing *m*-phenylenediamidate bridges.[3a] These results confirmed the previous assumptions that the electronic effects of the group linked to the *m*-phenylene moiety can tune the magnitude of the ferromagnetic interactions between the metal ions. Interestingly, the reaction of the dinuclear Ni^{2+} mesocate with Ln^{3+} ions allowed the preparation of the first examples of ferromagnetic Ni_2Ln cationic chain complexes.[3c] However, none of these systems exhibited single-chain magnet (SCM) behaviour.

As a part of our continuing work in this area,[3,4c] we have prepared two specifically designed ligands, H_2bpcb 1,3-bis(pyrimidine-2-carboxamide)benzene and H_2bpzcb 1,3-bis(pyrazine-2-carboxamide)benzene, which are closely related to the H_2mbpb ligand but having pyrimidine and pyrazine as terminal groups instead of pyridine. These ligands can also potentially form double and triple stranded dinuclear metallacyclic complexes showing ferromagnetic coupling between the metal ions. Moreover, these dinuclear complexes could coordinate metal ions not only through the carboxamide oxygen atoms, as observed for H_2mbpb complexes,[3] but also through the outward pyrimidine and pyrazine donor nitrogen atom oriented towards the external side of the mesocate. Therefore, they could be used as *synthons* to link other metal ions and form extended structures with new and original magnetic properties (Scheme 2). It should be noted at this point that during the course of this research a Ni_2 dinuclear mesocate complex based on the H_2bpzcb ligand was reported. As expected, this complex exhibits a ferromagnetic interaction between the metal ions, and interesting multi-electron oxidation processes.[6]

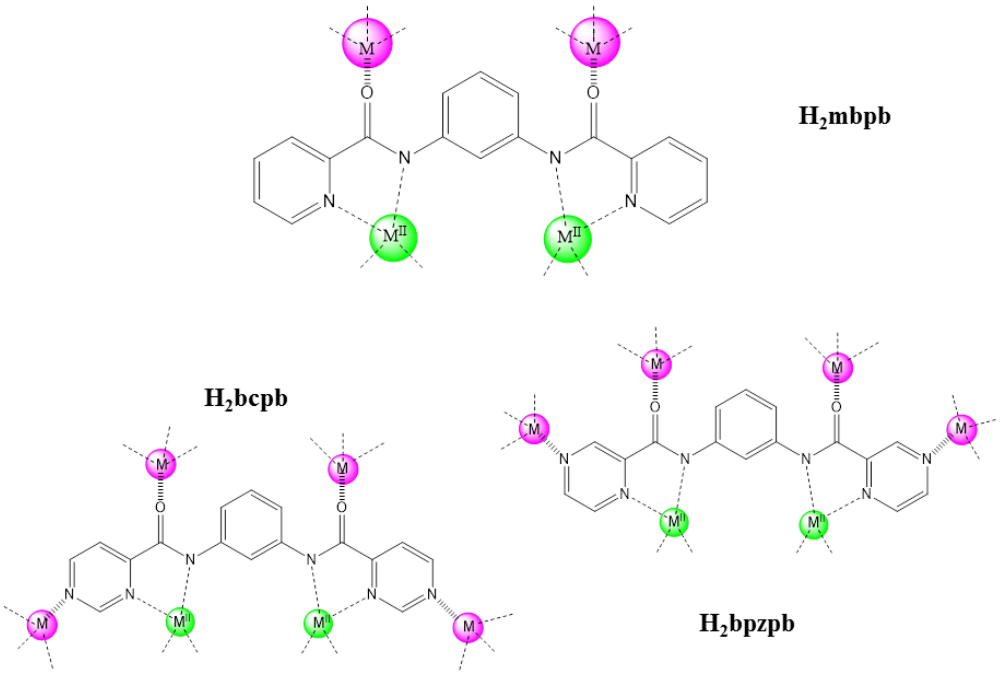

Scheme 2: Structure of the ligands H_2mbpb, H_2bcpb, H_2bpzpb and their potential coordination sites.

This paper reports the crystal structures, magnetic properties and theoretical calculations of Cu^{2+} and Ni^{2+} dinuclear mesocates with the H_2bcpb, H_2bpzpb ligands and their metal assembled Ni_2M (M^{2+} = Ni and Co) trinuclear, Ni_2Ln (Ln^{3+} = Tb and Gd) *zig-zag* chain and Ni_2Mn^{III} 2D honeycomb-like complexes.

Experimental Section

Materials

All analytical reagents were purchased from commercial sources and used without further purification. 4-pyrimidinecarboxylic acid was prepared according to a previously described procedure.[7]

Syntheses

Synthesis of 1,3-bis(pyrimidine-2-carboxamide)benzene (H_2bpcb) and 1,3-bis(pyrazine-2-carboxamide)benzene (H_2bpzcb)

H_2bpcb and H_2bpzcb were prepared following the general work-up reported by Mukherjee *et al.*[8] To a solution of 4-pyrimidinecarboxylic acid or 2-pyrazinecarboxylic acid (30 mmol) in pyridine (12 mL) was added *m*-phenylenediamine (15 mmol) in pyridine (10 mL). The mixture was stirred gently for 10 min and then triphenyl phosphite (30 mmol) was added slowly over a period of 15 min. The resulting solution was heated to 95 ºC with stirring for 4h, leading to a pale yellow solid which was filtered, washed with a small amount of cold pyridine, diethyl ether and air dried.

For H_2bpcb: Yield, 40%. Anal. Calcd. for $C_{16}H_{12}N_6O_2$: C, 60.00; H, 3.78; N, 26.24. Found: C, 60.25; H, 3.58; N, 26.38. IR (KBr pellet, cm^{-1}): 3339 ν (N-H), 3091 ν (C-H), 1699 ν (C=O); 1605 ν (C=C); 1530 ν (N-C). ^{1}H-NMR (d^6-DMSO, ppm): 10.82 (s, 2H), 9.42 (s, 2H), 9.13 (d, 2H), 8.56 (s, 1H), 8.13 (d, 2H), 7.63 (d, 2H), 7.37 (t, 1H).

For H_2bpzcb: Yield, 65%. Anal. Calcd. for $C_{16}H_{12}N_6O_2$: C, 60.00; H, 3.78; N, 26.24. Found: C, 60.14; H, 3.43; N, 25.90. IR (KBr pellet, cm^{-1}): 3295 ν (N-H), 3060 ν (C-H), 1682 ν (C=O); 1608 ν (C=C); 1544 ν (N-C). ^{1}H-NMR (d^6-DMSO, ppm): 10.72 (s, 2H), 9.28 (s, 2H), 8.92 (d, 2H), 8.80 (d, 2H), 8.55 (s, 1H), 7.59 (d, 2H), 7.34 (t, 1H).

Synthesis of complexes

$Na_{2.5}[Ni_2(bpcb)_3]\cdot 0.5OH\cdot 18.5H_2O$ (1)

To a suspension of H_2bpcb (0.1 g, 0.31 mmol) in hot water (20 mL) were successively added, under continuous stirring, two equivalents of NaOH (0.025 g, 0.62 mmol) and a solution of $Ni(NO_3)_2\cdot 6H_2O$ (0.060 g, 0.21 mmol) in 10 mL of water. The mixture was refluxed for 3h. Then, the unreacted ligand was filtered off. The resulting deep yellow solution was concentrated under vacuum. Addition of acetone causes precipitation of **1** as a yellow-brown powder. Single crystals suitable for X-ray diffraction were obtained by slow evaporation of a solution of the powder in a water/acetonitrile (2/1) mixture. Yield: 51 %. Anal. Calcd. for $C_{48}H_{67.5}N_{18}O_{25}Ni_2Na_{2.5}$: C, 39.18; N, 17.13; H, 4.62. Found: C, 39.32; N, 17.02; H, 4.24. IR (KBr pellet, cm^{-1}): 3422 ν(O-H), 1607 ν(C=O), 1580 ν(C=C), 1544 ν(C-N). The synthesis of **$(PPh_4)_2[Ni_2(bpcb)_3]$ (1')** was performed with the following method: to a solution of **1** (0.1 g, 0.081 mmol) in water (15 mL) were added two equivalents of $AgNO_3$ in water (10 mL), and the mixture was stirred for one hour at 60ºC. The resulting $Ag_2[Ni_2(bpcb)_3]$ solid was filtered, washed with water and dried in air. This solid was suspended in dichloromethane (10 mL) and two equivalents of PPh_4Cl in dichloromethane (10 mL) were added. The mixture was stirred for two hours and the precipitated AgCl filtered off. The filtrate containing the compound $(PPh_4)_2[Ni_2(bpcb)_3]$ was precipitated with diethyl ether, filtered, washed with diethyl ether and dried in air. Yield: 35%. Anal. Calcd. for $C_{96}H_{78}N_{18}O_6Ni_2P_2$: C, 65.55; N, 14.33; H, 4.47. Found: C, 65.79; N, 14.46; H, 4.34. IR (KBr, cm^{-1}): 3408, ν(OH); 3058, ν(CH); 1605, ν(C=O); 1579, ν(C=C); 1543, ν(CN).

$Na_2[Ni_2(bpzcb)_3]\cdot 16H_2O$ (2)

To a suspension of H_2bpzcb (0.640 g, 2 mmol) in water (30 mL) were successively added, under continuous stirring, a solution of NaOH (0.160g, 4 mmol) and a solution of $Ni(NO_3)_2\cdot 6H_2O$ (0.388 g, 1.33 mmol) in 10 mL of water. The mixture was refluxed for 2h, and then, the unreacted ligand was filtered off. The resulting amber solution was concentrated under vacuum. Addition of acetone causes precipitation of **2** as a yellow-brown powder. Yield: 65%. Anal. Calcd. for $C_{48}H_{62}N_{18}O_{22}Ni_2Na_2$: C, 40.99; N, 17.93; H, 4.44. Found: C, 40.57; N, 17.96; H, 4.03. IR (KBr pellet, cm^{-1}): 3412 ν(O-H), 1604 ν(C=O), 1570 ν(C=C) and ν(C-N).

$[Cu_2(bpcb)_2(H_2O)_2]\cdot 8H_2O$ (3)

NaOH (0.025 g, 0.62 mmol) and $Cu(NO_3)_2\cdot 3H_2O$ (0.075 g, 0.31 mmol) were successively added with continuous stirring to a hot aqueous solution (20 mL) of the H_2bpcb ligand (0.100g, 0.31 mmol) and the mixture refluxed for 3h. A crystalline dark-green precipitate was obtained, which was filtered off, washed with water and dried with acetone. Yield: 30%. Anal. Calcd. for $C_{32}H_{40}N_{12}O_{14}Cu_2$: C, 40.72; N, 17.81; H, 4.27. Found: C, 40.52; N, 18.15; H, 4.20. IR (KBr pellet, cm^{-1}): 3414, ν (O-H); 1604 ν(C=O); 1581, ν(C=C); 1544, ν(C-N).

$[Cu_2(bpzcb)_2(H_2O)_2]\cdot 4H_2O$ (4)

NaOH (0.040 g, 1 mmol) and $Cu(NO_3)_2\cdot 3H_2O$ (0.121 g, 0.5 mmol) were successively added with continuous stirring to an aqueous solution (20 mL) of the H_2bpzcb ligand (0.160g, 0.5 mmol), and the mixture refluxed for 2h. The resulting dark-green precipitate was filtered off, washed with water and dried with acetone. Yield: 70%. Anal. Calcd. for $C_{32}H_{28}N_{12}O_8Cu_2$: C, 45.99; N, 20.11; H, 3.38. Found: C, 45.76; N, 19.96; H, 3.19. IR (KBr pellet, cm^{-1}): 3387, ν (O-H); 1604 ν(C=O); 1572, ν(C=C); and ν(C-N).

$[Ni(H_2O)_5Ni_2(bpcb)_3]\cdot 18H_2O$ (5)

To a solution of **1** (0.1g, 0.081 mmol) in a mixture of water/acetonitrile (1/1) under stirring was added dropwise a solution of $Ni(ClO_4)_2\cdot 6H_2O$ (0.089 g, 0.24 mmol) in the same mixture of solvents. The resulting yellow-brown solution was allowed to stand at room temperature and partial evaporation of the solvent resulted in a crop of deep-yellow crystals that were filtered off, washed with a minimal amount of water, acetone and dried *in vacuo*. Yield: 40 %. Anal. Calcd. for $C_{48}H_{76}N_{18}O_{29}Ni_3$: C, 37.31; N, 16.32; H, 4.96. Found: C, 37.00; N, 16.12; H, 4.36. IR (KBr pellet, cm^{-1}): 3388 ν(O-H), 1604 ν(C=O), 1573 ν(C=C), 1544 ν(C-N).

$[Co(H_2O)_5Ni_2(bpcb)_3]\cdot 15H_2O$ (6)

This complex was obtained following the same synthetic procedure described above for complex **5** but using $Co(ClO_4)_2\cdot 6H_2O$ (0.090 g, 0.24 mmol) as the metallic salt added to **1**. Yield: 38 %. Anal. Calcd. for $C_{48}H_{70}N_{18}O_{26}Ni_2Co$: C, 38.65; N, 16.90; H, 4.73. Found: C, 38.91; N, 16.72; H, 4.42. IR (KBr pellet, cm^{-1}): 3388 ν(O-H), 1604 ν(C=O), 1573 ν(C=C), 1544 ν(C-N).

$(PPh_4)\{[Ni_2(bpcb)_3]_2[Mn(acen)]_3\}$ (7)

A solution of [Mn(acen)Cl][9] (acen = N, N'-ethylenebis(acetylacetonateiminate)) (0.036 g, 0.116 mmol) in acetonitrile (15 mL) was added to a solution of $(PPh_4)_2[Ni_2(bpcb)_3]$ (**1'**) (0.05 g, 0.029 mmol) in acetonitrile (10 mL) and the mixture stirred for 30 minutes. The slow diffusion of diethylether into the mother liquor at room temperature afforded single crystals suitable for X-ray diffraction. Yield: 10%. Anal.Cald for

$C_{156}H_{134}N_{42}O_{18}Ni_4Mn_3P$: C, 56.51; H, 4.07; N, 17.74. Found: C, 56.12; H, 3.77; N, 17.72. IR (KBr, cm^{-1}): 3399, ν(OH); 1604, ν(C=O); 1574, ν(C=C); 1543, ν(CN).

$[\{[Ni_2(bpzcb)_3]Tb(H_2O)_5\}(CF_3SO_3)\cdot THF\cdot 5H_2O]_n$ (8)

Compound **8** was obtained by slow diffusion of a water solution (3 mL) of $Tb(CF_3SO_3)_3$ (0.065 g, 0.108 mmol) into a 3 mL solution of **2** (0.025 g, 0.018 mmol) through a 3 mL tetrahydrofuran (THF) layer in a 2.5-cm diameter glass tube. After several days amber quality crystals of **8** formed. Yield: 19%. Anal. Calcd for $C_{55}H_{55}N_{16}O_{15.5}Ni_2TbSF_3$: C, 42.52; H, 3.57; N, 14.43; S, 2.06. Found: C, 42.55; H, 3.06; N, 14.55; S, 2.23. IR (KBr,cm-1): 3224, ν(O-H); 1601, ν(C=O); 1566, ν(C=C) y ν(C-N); 1289, 1222, ν(CF_3SO_3).

$[\{[Ni_2(bpzcb)_3]Gd(H_2O)_4(NO_3)\}\cdot 2THF\cdot 3H_2O]_n$ (9)

This complex was synthesised following the same procedure as that for **8** but using $Gd(NO_3)_2\cdot 5H_2O$ (0.047 g, 0.108 mmol). Yield: 12%. Anal. Calcd for $C_{56}H_{52}N_{19}O_{18}Ni_2Gd$: C, 43.29; H, 3.37; N, 17.13. Found: C, 42.96; H, 4.03; N, 16.74. IR (KBr,cm-1): 3424, ν(O-H); 2983, ν(C-H); 1600, ν(C=O); 1562, ν(C=C) y ν(C-N); 1382, ν(NO_3).

$[\{[Ni_2(bpzcb)_3]Tb(H_2O)_4(NO_3)\}\cdot 2THF\cdot 6H_2O]_n$ (10)

This complex was synthesised following the same procedure as that for **8** but using $Tb(NO_3)_2\cdot 5H_2O$ (0.037 g, 0.108 mmol). Yield: 20%. Anal. Calcd for $C_{56}H_{58}N_{19}O_{21}Ni_2Tb$: C, 41.79; H, 3.63; N, 16.54. Found: C, 42.32; H, 3.42; N, 16.64. IR (KBr,cm-1): 3423, ν(O-H); 1600, ν(C=O); 1563, ν(C=C) y ν(C-N); 1379, ν(NO_3).

Physical Measurements

Elemental analyses were carried out at the "Centro de Instrumentación Científica" (University of Granada) on a Fisons-Carlo Erba analyser model EA 1108. IR spectra on powdered samples were recorded with a ThermoNicolet IR200FTIR by using KBr pellets. ^1H NMR spectra were obtained using a Bruker ARX400 spectrometer. Chemical shifts are reported in δ units (parts per million) downfield from TMS. Magnetisation and variable temperature (2-300 K) magnetic susceptibility measurements on powdered crystalline samples were carried out with a Quantum Design SQUID MPMS XL-5 using a magnetic field of 0.1 T. Field dependent magnetisation measurements were carried out at different temperatures in the field range 0-5 T. The experimental susceptibilities were corrected for the diamagnetism of the constituent atoms by using Pascal's tables.

X-Ray Crystallography

Suitable single crystals were mounted on a glass fibre and used for data collection on Bruker APEX CCD (**1, 3, 4, 5**), Oxford diffraction super nova (**7**) and Xcalibur 2 (**8-10**) diffractometers at 298 K (**3**) 293 K (**4, 9, 10**), 273 K (**1, 5**), 100 K (**7**) and 170 K (**8**) using graphite monochromated Mo Kα radiation (λ = 0.71073 Å). The structures were solved by direct methods and refined with full-matrix least-squares calculations on F^2

using the program SHELXS97.[10] All non-hydrogen atoms were refined anisotropically while the hydrogen atoms were calculated and therefore included as isotropic fixed contributors to F_c.

In the case of compound **5**, the hydrogen atoms associated with the lattice water molecules, O16W and O17W, could not be directly located from difference Fourier maps. Crystals of complexes **6** and **8** underwent fast and severe degradation such that the diffraction data were too weak as to permit a complete refinement and an accurate description of the structure. However both structures were partially refined. For **6**, the unit cell parameters and partial refinement confirmed that the complex is isostructural to **5**. In the case of **8**, the anisotropic model was only applied to the metal ions while the rest of atoms were considered isotropically. Details of data collections and refinements are given in Table 1. All attempts to consider the disorder of the PPh_4^+ cation in compound **7** failed. Instead, a new set of F2 (hkl) values with the contribution from this cation withdrawn, was obtained by the SQUEEZE procedure implemented in PLATON-94.[11] The CCDC no. of the crystal structures (1411914 for **7** and 1551794-1551800 for **4, 9, 8, 10, 1, 3** and **5**, respectively) contains the supplementary crystallographic data for this paper.

Results and discussion

The ligands H_2bpcb and H_2bpzcb were synthesised by coupling two equivalents of diazine carboxylic acid (4-pyrimidinecarboxilic acid or 2-pyrazinecarboxilic), with one equivalent of 1,3-phenylenediamine following the synthetic protocol reported by Mukherjee *et al.* that uses pyridine as solvent and Ph_3P as dehydrating agent.[8] These ligands react with NaOH and $Ni(NO_3)\cdot 6H_2O$ (in a 3:6:2 molar ratio) to afford dinuclear triple stranded anionic complexes of formula $Na_{2.5}[Ni_2(bpcb)_3]\cdot 0.5OH\cdot 18.5H_2O$ (**1**) and $Na_2[Ni_2(bpzcb)_3]\cdot 16H_2O$ (**2**), where the amide groups of the ligand are fully deprotonated. The reaction of $Ag_2[Ni_2(bpcb)_3]$ (which was prepared from **1** and $AgNO_3$ in water) with two equivalents of PPh_4Cl in dichloromethane led to $(PPh_4)_2[Ni_2(bpcb)_3]$ (**1'**). Reaction of the ligands with Cu^{2+} ions under the same conditions as for **1** and **2**, but using instead a 1:2:1 molar ratio, led to dinuclear neutral double stranded complexes of formulae $[Cu_2(bpcb)_2(H_2O)_2]\cdot 3H_2O$ (**3**) and $[Cu_2(bpzcb)_2(H_2O)_2]\cdot 2H_2O$ (**4**). Following the "complex as ligand" strategy, the dinuclear $[Ni_2(L)_3]^{2-}$ (L = bpcb and bpzcb) units of **1**, **1´**and **2** were used as building blocks to be assembled with transition and rare earth metal ions to afford unusual homo- and heterometallic species. Thus, the reaction of **1** in aqueous medium with perchlorate salts of M^{2+} [M^{2+} = Ni and Co] led to the formation of neutral, bent, trinuclear molecules of general formula $[M^{II}Ni^{II}_2(bpcb)_3]\cdot xH_2O$ (**5** and **6**). The assembly of **1'** with Mn(acen)Cl in acetonitrile afforded the 2D honeycomb-like complex $(PPh_4)\{[Ni_2(bpcb)_3]_2[Mn(acen)]_3\}$(**7**). Finally, using complex **2** as building block only 1D $[Ni_2Ln]_n$ structures of formulae $[\{[Ni_2(bpzcb)_3]Tb(H_2O)_5\}(CF_3SO_3)\cdot THF\cdot 5H_2O]_n$ (**8**) and $[\{[Ni_2(bpzcb)_3]Ln(H_2O)_4(NO_3)\}\cdot 2THF\cdot xH_2O]_n$ (Ln^{3+} = Gd, x =3 (**9**) and Tb, x= 6 (**10**)) could be obtained. It is worth mentioning at this point that complexes **5**, **6** and **7** contain a pyrimidine bridging group connecting one of the Ni^{2+} ions of the $[Ni_2(bpcb)_3]^{2-}$ building block and either one M^{2+} (M^{2+}= Ni, Co) or Mn^{3+} ion. It should also be noted, that other magnetically interesting Ln^{3+} ions such as Dy^{3+}, Yb^{3+} and Ho^{3+} were used but in no case were suitable quality single-crystals for X-ray crystallography

obtained. Finally, all attempts to obtain polynuclear species using compounds **3** and **4** as building blocks failed, probably due to their neutral nature and low solubility.

Crystal structures

The structure of **1** contains a triple stranded metallacyclic $[Ni_2(bpcb)_3]^{2-}$ anion, where the Ni^{2+} ions are bridged by three fully deprotonated bisbidentate ligands (Figure 1), with charge balanced maintained through the presence of octahedral $[Na(H_2O)_6]^+$ cations.

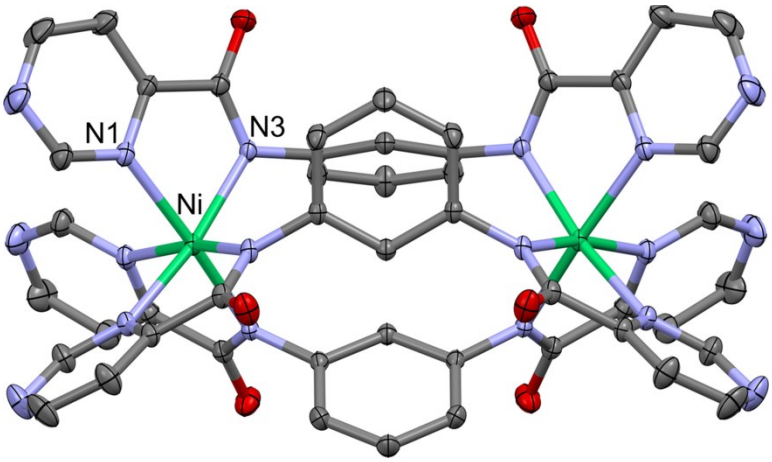

Figure 1: Perspective view of the structure of the anion of **1**. H atoms and counter cations have been omitted for the sake of clarity. Ellipsoids are drawn at 30 % probability.

Within the $[Ni_2(bpcb)_3]^{2-}$ moiety, the symmetry related Ni^{2+} ions exhibit a distorted NiN_6 coordination environment, formed by coordination in a *fac* disposition of three pyrimidine (N1) and three amidate (N2) nitrogen atoms belonging to three different $bpcb^{2-}$ ligands. This coordination sphere shows a trigonally distorted octahedral geometry. The Ni-N1 and Ni-N3 bond distances are 2.119(2) Å and 2.083(2) Å respectively. *cis*-N1-Ni-N1, *cis*-N1-Ni-N3 and *cis*-N3-Ni-N3 bond angles are 91.46(9)º, 78.03(9)º and 98.92(8)º respectively, whereas the *trans*-N1-Ni-N3 bond angle is 168.98(9)º. The intramolecular Ni-Ni distance is 6.858(1) Å while the shorter intermolecular Ni····Ni distance is 8.8735(4) Å. The two octahedral NiN_6 coordination environments exhibit opposite chirality (Δ and Λ, Figure S1) and consequently, the $[Ni_2(bpcb)_3]^{2-}$ metallacycle anion is a meso-helicate with pseudo-C_{3h} symmetry, the three-fold axis lying on the line connecting the two Ni^{2+} ions and the horizontal plane of symmetry passing through half of the central benzene rings.

The bpcb ligand exhibits a non-planar conformation, the dihedral angle between the benzene and pyrimidine ring mean planes being 87.20(12)º. The *m*-phenylene rings are face-to-edge π stacked with those on adjacent ligands strands, leading to C-H····π interactions with C-centroid distances of 3.234(4) Å.

The dinuclear unit in **1** is very similar to those previously reported for the complexes $[Ni_2(mbpb)_3]PF_6 \cdot 21H_2O$[3b] and $(nBu_4N)_2[Ni(bpzcb)_3] \cdot 4MeOH$.[6]

Table 1: Crystallographic data and structural refinement details for compounds **1, 3-5, 8-11**.

Compound	**1**	**3**	**4**	**5**	**7**	**8**	**9**	**10**
chemical formula	$C_{48}H_{67.5}N_{18}Na_{2.5}Ni_2O_{25}$	$C_{32}H_{40}N_{12}Cu_2O_{14}$	$C_{32}H_{28}N_{12}Cu_2O_8$	$C_{48}H_{76}N_{18}Ni_3O_{29}$	$C_{180}H_{144}N_{42}O_{18}P_2Ni_4Mn_3$	$C_{55}H_{55}N_{16}O_{15.5}Ni_2TbF_3S$	$C_{52}H_{53}N_{19}O_{17.5}Ni_2Gd$	$C_{52}H_{53}N_{19}O_{17.5}Ni_2Tb$
M/gmol^{-1}	1471.59	943.84	835.74	1545.39	3645	1553.55	1498.8	1500.5
cryst syst	hexagonal	monoclinic	Triclinic	monoclinic	Triclinic	monoclinic	monoclinic	monoclinic
space group	$P6_3/m$	C2/c	P-1	$P2_1/c$	P-1	$P2_1/n$	$P2_1/c$	$P2_1/c$
a/ Å	13.9631(4)	23.397(6)	7.6178(19)	13.076(3)	18.933(4)	11.001(5)	13.390(7)	13.282(6)
b/ Å	13.9631(4)	11.832(3)	11.658(3)	20.453(4)	20.478(4)	28.854(5)	24.953(9)	24.900(8)
c/ Å	21.1354(14)	15.243(4)	11.819(3)	24.811(5)	25.275(5)	18.858(5)	20.781(10)	20.701(8)
α/deg	90	90	116.89(5)	90	92.019(16)	90	90	90
β/deg	90	99.617(5)	100.69(5)	96.72(3)	98.658(17)	101.021(5)	107.632(5)	107.98(5)
γ/deg	120	90	101.23(5)	90	104.52(16)	90	90	90
V/ Å^3	3568.7(3)	4160.3(18)	872.2(4)	6590(2)	9351(3)	5876(3)	6616.9(6)	6514.3(5)
Z	2	4	1	4	2	4	4	4
ρ(g cm^{-3})	1.369	1.507	1.591	1.558	1.295	1.756	1.505	1.530
μ(mm^{-1})	0.627	1.100	1.289	0.947	2.772	1.955	1.633	1.726
R1[a] [I>2σ(I)]	0.0524	0.0749	0.0807	0.0935	0.0525	0.0470	0.0648	0.0643
wR2[a] [I>2σ(I)]	0.1582	0.1742	0.1881	0.1697	0.1457	0.1156	0.1604	0.1680

The structures of **3** and **4** are similar and can be described as neutral dinuclear molecules, withwater molecules of crystallisation (Figure 2).

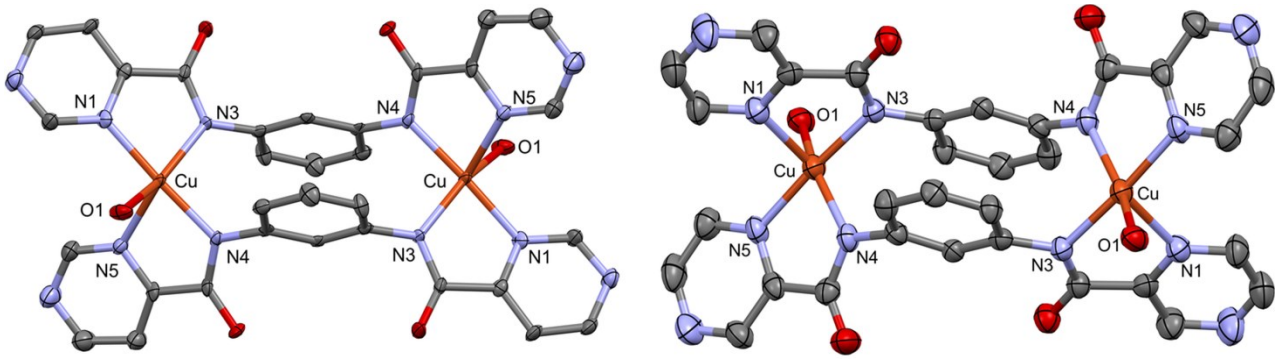

Figure 2: Structures of compounds **3** and **4**. Hydrogen atoms and water molecules of crystallisation are omitted for clarity. Ellipsoids are drawn at 50 % probability.

In each dinuclear structure, the Cu^{2+} ions are bridged by two bisbidentate ligands through the nitrogen atoms of amide group (Cu-N3 = 1.974(5) Å and Cu-N4 = 1.971(5) Å for **3** and Cu-N3 = 1.980(5) Å, Cu-N4 = 1.990(5) Å for **4**) and one of the nitrogen atoms of either the pyrimidine or pyrazine rings, respectively, with bond distances of Cu-N1 = 2.003(6) Å and Cu-N5 = 2.195(6) Å for **3** and Cu-N1 = 2.152(5) Å and Cu-N5 =

2.013(5) Å for **4**. The Cu^{2+} coordination sphere is completed with a coordinated water molecule, with a Cu-O bond distance of 2.041(5) Å for **3** and 2.105(4) Å for **4**, leading to a distorted square pyramidal geometry for the CuN_4O coordination environment in both cases. Using Addison's method,[12] the τ values for **3** and **4** are 0.47 and 0.45, respectively, which indicate an intermediate geometry between trigonal bipyramid, TBPY-5, and square-pyramid, SPY-5, (τ = 1 for a trigonal bipyramidal geometry, and τ = 0 for a square based pyramidal geometry). The intramolecular Cu-Cu distance is 7.436(2) Å for **3** and 7.4523(18) Å for **4**, while the shortest intermolecular Cu···Cu distance is 7.5221(16) Å for **3** and 7.130(2) Å for **4**.

The benzene rings sit parallel to each other, but mutually shifted, adopting an *anti* conformation with a distance of 3.924(5) Å for **3** and 3.483(5) Å for **4**, preventing any π–π interactions between the rings. As in **1**, the ligands exhibit a non-planar conformation with two different dihedral angles between the benzene and pyrimidine/pyrazine ring mean planes, which are 50.36(2)º and 85.19(2)º for **3** and 68.21(2)º and 21.45(2)º for **4**. In both cases, the coordinated water molecules and water molecules of crystallisation are involved in hydrogen bonding interactions between each other and oxygen atoms of the ligands. Moreover, in the case of **3** the nitrogen atoms of the ligands also participate in hydrogen bonding interactions with crystallization water molecules (Figure S2). The extensive hydrogen bonding 3D network thus generated exhibits donor-aceptor distances in the 2.668 Å - 2.880 Å and 2.745 Å - 2.821 Å rages, for **3** and **4**, respectively.

In the structure of **5**, the $[Ni_2(bpcb)_3]^{2-}$ dinuclear mesocate unit is linked to one Ni^{II} ion through the outward nitrogen atom of one pyrimidine ring, thus resulting in a unique, neutral, bent trinuclear molecule (Figure 3). The fact that the molecule is neutral, as well as the weak basic character of the external nitrogen atom of the pyrimidine rings, could be the reason that an extended structure is not formed.

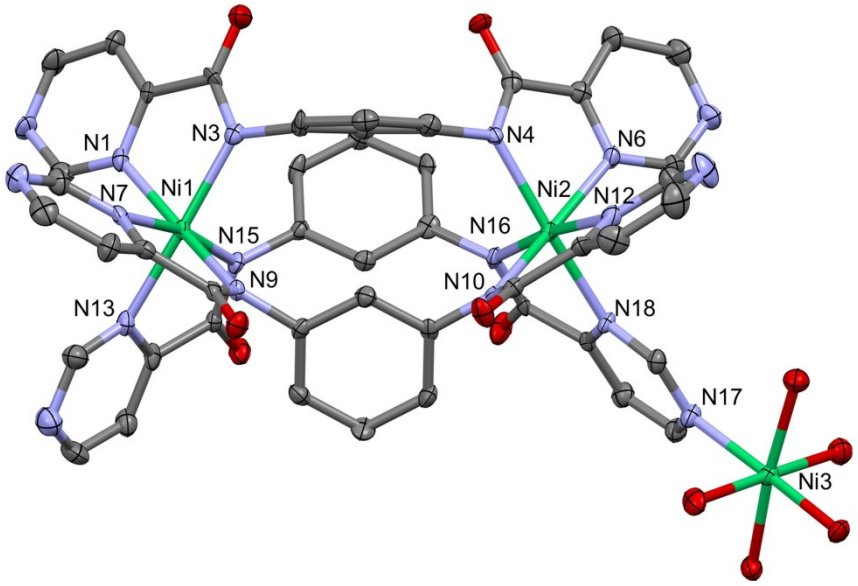

Figure 3: X-ray crystal structure of the metal complex of **5**. Water molecules of crystallisation and hydrogen atoms have been omitted for clarity. Ellipsoids are drawn at 50 % probability.

As expected for the $[Ni_2(bpcb)_3]^{2-}$ unit, the structural parameters are similar to those found in **1**. The Ni1 and Ni2 ions exhibit slightly distorted octahedral NiN_6 coordination environments formed by three nitrogen atoms belonging to the amide group and three atoms of the pyrimidine rings. The $Ni\text{-}N_{amide}$ and $Ni\text{-}N_{pyrimidine}$ bond lengths vary between 2.066(5)-2.085(5) Å and 2.076(5)-2.106(5) Å for Ni1, and 2.068(5)-2.106(5) Å and 2.111(5)-2.147(5) Å for Ni2, respectively. *Cis*-$N_{pyrimidine}$-Ni-$N_{pyrimidine}$, N_{amide}-Ni-$N_{pyrimidine}$ and N_{amide}-Ni-N_{amide} bond angles are in the ranges of 91.97(18)º-96.69(19)º, 76.57(18)º-78.30(19)º and 94.53(18)º-100.72(19)º respectively. *Trans*- N_{amide}-Ni-$N_{pyrimidine}$ bond angles are close to linearity (167.76(18)º-173.35(18)º). The Ni1-Ni2 distance is 6.8984(17) Å, which is similar to that found in the precursor **1**. The mean value of the dihedral angle between the phenyl and pyrimidine rings is 79.98(19)°. Ni3 exhibits a NiN_5O coordination environment, which is formed by five oxygen atoms belonging to five water molecules and one nitrogen atom from a pyrimidine ring, giving rise to a distorted octahedron around the metal ion with approximate C_{4v} symmetry [the main factor accounting for this distortion is the N17-Ni3 distance (2.118(5) Å), which is considerably longer than the Ni3-O bond distances (2.043(4)-2.067(4) Å)]. The oxygen atoms of the amidate groups and the water molecules coordinated to Ni3 are again all involved in a myriad of hydrogen bonding interactions with a great number of water molecules of crystallisation, which contributes to the stabilisation of the molecular packing (Figure S3).

The asymmetric unit of the crystal structure of **7** contains two anionic, dinuclear $[Ni_2(bpcb)_3]^{2-}$ units (made of the metallic atoms Ni1/Ni4 and Ni2/Ni3), three cationic $[Mn(acen)]^+$ units (Mn1, Mn2 and Mn3) and one PPh_4^+ cation. (Figure 4)

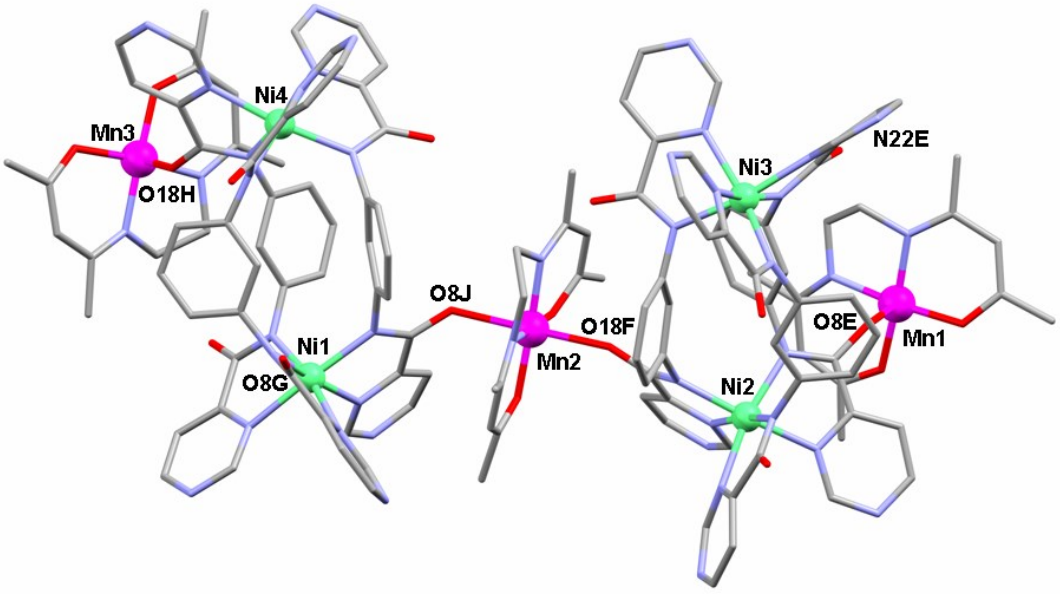

Figure 4: Asymmetric unit of the structure of **7**.

For each $[Ni_2(bpcb)_3]^{2-}$ unit, the bond angles and distances, the disposition of the bpcb ligands and the coordination sphere of the Ni(II) ions are quite similar to those observed in compound **1**. The Ni1-Ni4 and Ni2-Ni3 distances are 6.856(7) Å and 6.880(7) Å, respectively, whereas the mean value of the dihedral angle

between the phenyl and pyrimidine rings is 77.19(13)°. In the $[Mn(acen)]^+$ units, the Mn(III) ion presents a Jahn-Teller distorted octahedral coordination environment with equatorial distances in the range of 1.916(2)-1.986(3) Å for Mn1, 1.914(3)-1.993(3) Å for Mn2 and 1.918(2)-1.979(3) Å for Mn3, and axial distances in the range of 2.168(3)-2.172(3) Å for Mn1, 2.203(2)-2.234(2) for Mn2 and 2.101(2)-2.427(2) Å for Mn3.

Each Ni_2 mesocate unit is linked to three different $[Mn(acen)]^+$ units. Specifically, the anionic Ni^{2+} unit containing the Ni1 and Ni4 ions is joined to three Mn(III) ions through the oxygen atom of one amide group belonging to each bpcb ligand with bond distances of Mn1-O8G, Mn2-O8J and Mn3-O18H, 2.168(3) Å, 2.203(2) Å and 2.101(2) Å, respectively (Figure 4).

In the case of the anionic Ni_2 mesocate unit containing the Ni2 and Ni3 ions, the Mn1 and Mn2 ions are also linked to the oxygen atoms of the amide group of two different bpcb ligands with bond distances Mn1-O8E and Mn2-O18F of 2.172(3) Å and 2.234(2) Å, respectively. However, Mn3 is joined to the outward N22 nitrogen atom of the pyrimidine ring belonging to the bpcb ligand that is also coordinated to Mn1 with a Mn3-N22 distance of 2.428(2) Å.
If the Ni2 units are considered as spacers and the Mn^{3+} ions as nodes, this connectivity gives rise to a (6, 3) *honeycomb* corrugated layered structure extended in the *ab* plane (Figure 5). Each hexagonal ring is formed by six $[Ni_2(bpcb)_3]^{2-}$ dinuclear units and six $[Mn(acen)]^+$ cations, which alternate, so that the former occupy the vertices and the latter are located on the edges of the hexagon (Figures 5 and S4). The corrugated layers are shifted with respect to each other, and interdigitated in such a way that the $[Ni_2(bpcb)_3]^{2-}$ dinuclear units and $[Mn(acen)]^+$ cations in the ridges above and below one layer are oriented toward the grooves formed by the same units in the neighbouring layers, ultimately leading to an ABAB sequence of layers stacked along the crystallographic *c* axis (Figure S5).

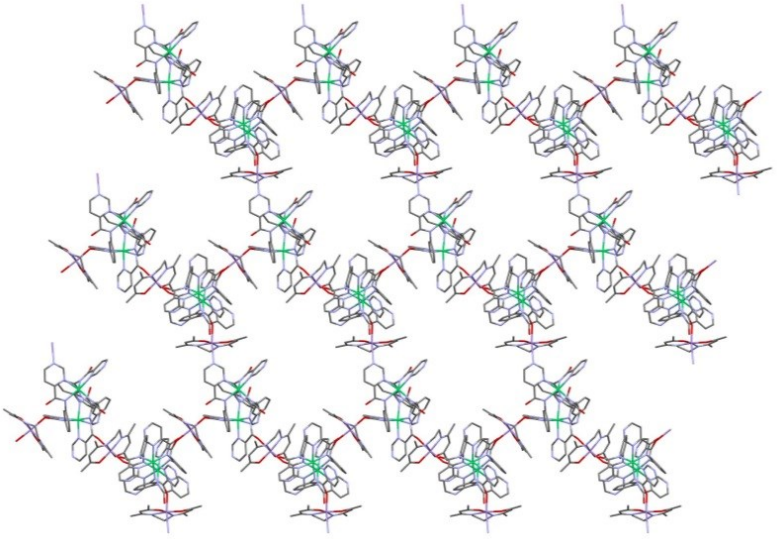

Figure 5: Projection of the 2D *honeycomb* structure of **7** along the [001] direction

The structure of **8** consists of cationic chains extended along the [101] direction of the crystal, formed by dinuclear $[Ni_2(bpzcb)_3]^{2-}$ units joined to Tb^{3+} ions through one of the amidate groups of two different ligands,

a triflate counter anion, and THF and water molecules of crystallisation (Figure 6). Within the chains, the Tb^{3+} ions are linked to the dinuclear $[Ni_2(bpzcb)_3]^{2-}$ through the oxygen atoms of two different bpzcb ligands with Tb-O bond distances of 2.219(8) and 2.230(8) Å. Likewise, the Tb^{3+} ions adopt a *zig-zag* conformation along the chain with an Tb-Tb-Tb angle of 120(3)º and a Tb···Tb distance of 10.077(9) Å.

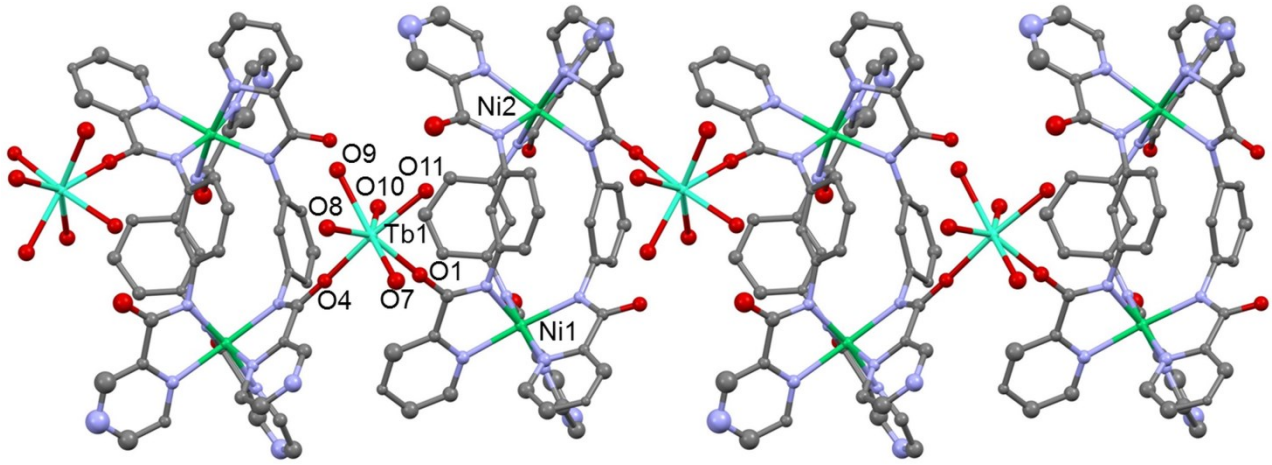

Figure 6: Structure of the cationic chain in **8**. Hydrogen atoms-are omitted for clarity.

The coordination sphere of the Tb^{3+} ions is completed with five water molecules, leading to a TbO_7 coordination sphere with Tb-O_{water} distances in the range of 2.351(8)-2.379(8) Å. Calculations of the degree of distortion of the TbO_7 coordination sphere with respect to an ideal seven-vertex polyhedron using continuous shape measure theory and SHAPE software,[13] indicate that the TbO_7 coordination polyhedron can be considered as intermediate between pentagonal bipyramid (PBPY-7), capped trigonal prism (CTPR-7) and capped octahedron (COC-7), with shape measure values 1.06, 2.94 and 4.42, respectively. In this arrangement, the oxygen atoms belonging to the amidate groups occupy one axial and one equatorial position, adopting a *cis* conformation. The *cis*-O-Tb-O angles are in the range of 70.46(3)-75.25(3)º whereas the *trans*-O-Tb-O angle is 174.1(3)º.

At a supramolecular level (see Figure S6), the free oxygen atoms of the bpzcb ligands belonging to one chain and the water molecules coordinated to the Tb^{3+} ions belonging to a neighbouring chain are involved in hydrogen bonding interactions to form a 2D system with donor-acceptor distances in the range 2.574(8)-2.867(8) Å. In addition, free and coordinated water molecules, as well as triflate anions, are also involved in hydrogen bond interactions, ultimately giving rise to a 3D network (Figure S7).

Compounds **9** and **10** are isostructural and consist of neutral chains of formula $\{[Ni_2(bpzcb)_3]Ln(H_2O)_4(NO_3)\}_n$, two tetrahydrofuran molecules with half occupancy and several water molecules of crystallisation (Figure 8).

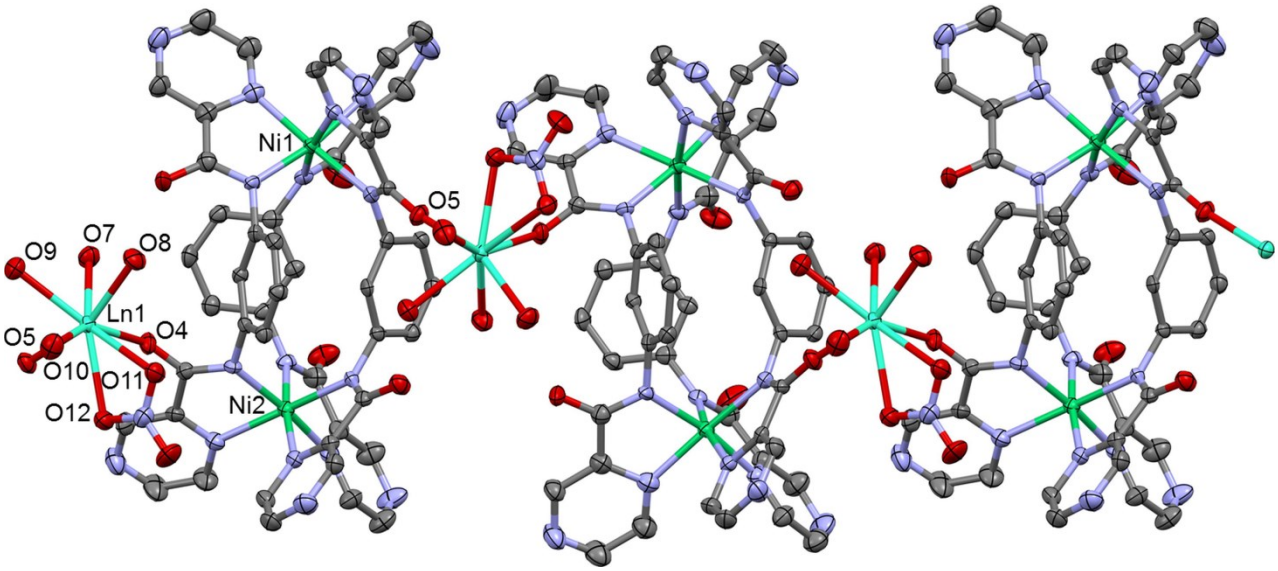

Figure 8: Structure of compounds **9** (Ln = Gd^{III}) and **10** (Ln = Tb^{III}). Hydrogen atoms and solvent molecules are omitted for clarity. Ellipsoids are drawn at 50 % probability.

The $[Ni_2(bpzcb)_3]^{2-}$ unit acts as a bidentate bridging ligand connecting the Ln^{3+} ions through two oxygen atoms of two different ligands, leading to a *zig-zag* conformation along the chain with Ln-Ln-Ln angles of 100.3(17)° and 100.6(16)° for **9** and **10**, respectively. The remaining sites of the Ln^{3+} ion are saturated by four water molecules and one nitrate anion affording a LnO_8 coordination environment. Continuous shape measurements indicate that the LnO_8 coordination polyhedron is intermediate between various ideal polyhedra, but closer to trigonal dodecahedron (TDD-8). The lowest shape measures correspond to trigonal dodecahedron (TDD-8), snub diphenoid (JSD-8) and biaugmented trigonal prism (BTPR-8) with values of 2.030, 2.309 and 3.033, respectively, for **9** and 2.045, 2.259 and 2.943, respectively, for **10**.

Although **9** and **10** are similar to **8**, the use of nitrate salts of lanthanides instead of trifluoromethanesulfonate in the syntheses, gives rise to some important structural differences: (i) the Ln coordination environment is LnO_8 dodecahedral for **9** and **10** and LnO_7 trigonal bipyramid for **8**. For the former, the Ln^{3+} ions are coordinated by two oxygen atoms belonging to ligands of two different dinuclear units (with Ln-O bond distances of 2.255(4) and 2.269(5) Å for **9** and 2.231(5) and 2.251(4) for **10**), water molecules (with Ln-O distances in the range 2.365(5)-2.449(5) Å for **9** and 2.314(5)-2.429(5) Å for **10**) and one nitrate anion (with distances of 2.522(5) and 2.529(5) Å for **9** and 2.503(5) and 2.513(5) Å for **10**); (ii) The Ln-O bond distances for complexes **9** and **10** are longer than those observed for **8**, and therefore, the Ln-Ln distances are also longer (10.5515(5) Å and 10.5114(4)Å). However, the Ni-Ni distances for **9** and **10** are shorter than that found in **8**, which can be attributed to a bigger distortion of the $[Ni_2(bpzcb)_3]^{2-}$ in the former (in all these chain compounds the dinuclear Ni_2 units are distorted and no longer present the three-fold axis and the plane perpendicular to this axis); iii) The Ln-Ln-Ln angles for **9** and **10** (100.3(17)º and 100.6(16)º, respectively) are smaller than for compound **8** (120(3)°); (iv) In **9** and **10**, the carboxamide oxygen atoms of the ligands, the water molecules coordinated to the Ln^{3+} ions, as well the free water molecules are involved

in hydrogen bonding interactions, but at variance with compound **8**, do not exhibit interchain interactions (Figure S8).

All attempts to obtain polynuclear species with pyrazine-bridged moieties similar to compounds **5-7** were unsuccessful, which may be due to the lower basicity of pyrazine compared to pyrimidine rings (the pK_b values for pyrazine and pyrimidine are 13.49 and 12.77, respectively).

Magnetic properties

The magnetic properties of **1** and **2** are given in Figure 9 and Figure S9, respectively, in the form $\chi_M T$ vs T (χ_M is the molar magnetic susceptibility per Ni_2 unit), measured under a constant magnetic field of 0.1 T in the 2−300 K. range. At room temperature the $\chi_M T$ values of 2.35 cm^3 K mol^{-1} for **1** and 2.37 cm^3 K mol^{-1} for **2** match well with the expected value for two uncoupled Ni^{2+} ions (S = 1) with g = 2.16 for **1** and 2.18 for **2**. When the temperature is lowered from room temperature, $\chi_M T$ steadily increases to reach a maximum of 2.84 cm^3 K mol^{-1} at 6 K for **1** and 2.83 cm^3 K mol^{-1} for **2** at 5 K, suggesting the existence of ferromagnetic coupling between the Ni^{2+} ions through the bpcb and bpzcb bridging ligands in **1** and **2**, respectively. The $\chi_M T$ value at the maximum is smaller than the theoretical value expected for two ferromagnetically coupled Ni^{2+} ions with an S = 2 ground state (3.53 cm^3Kmol^{-1} with g = 2.17). Below the temperature of the maximum, $\chi_M T$ decreases due to zero-field splitting (ZFS) and/or antiferromagnetic interactions between adjacent dinuclear entities.

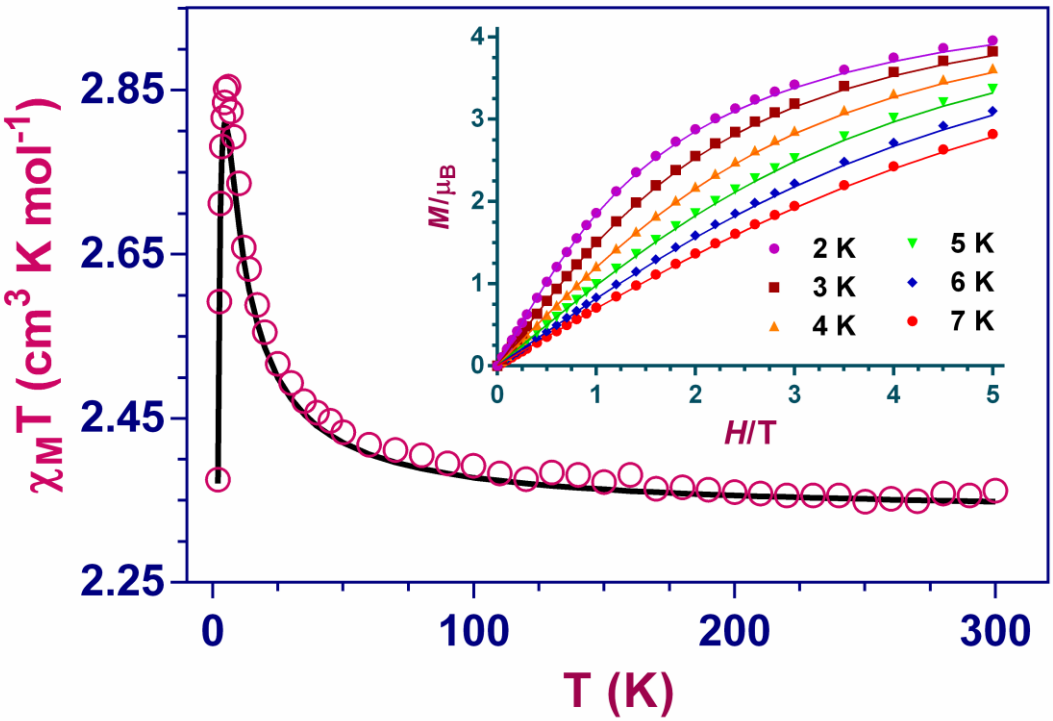

Figure 9: Temperature dependence of the $\chi_M T$ product for **1.** Inset: Field dependence of the magnetisation at different temperatures. Solid lines represent the best fit with the parameters indicated in the text, with

zJ' fixed at zero.

The magnetic susceptibility data were modelled with the following Hamiltonian:

$$\widehat{\boldsymbol{H}} = -J\widehat{\boldsymbol{S}}_{Ni1}\widehat{\boldsymbol{S}}_{Ni2} + D_{Ni}\left(\widehat{\boldsymbol{S}}^2_{Ni1z} + \widehat{\boldsymbol{S}}^2_{Ni2z}\right) + g\beta H(S_{Ni1} + S_{Ni2}) - zJ'\langle S_z\rangle \qquad \text{eq. 1}$$

The first term represents the isotropic exchange coupling, the second term the local zero-field splitting of the Ni^{2+} ions, the third term the Zeeman interaction, and the last term takes into account intermolecular interactions using the mean-field approach. The best simultaneous fitting of the temperature dependence of magnetic susceptibility and field dependence of magnetisation at different temperatures with the above Hamiltonian using the full-matrix diagonalization PHI program[14] and fixing $zJ' = 0$ afforded the following set of parameters: $J = +2.0$ cm^{-1}, $D = 4.0$ cm^{-1} and $g = 2.16$ for **1** {$R = 7.5x10^{-5}$ ($R = \Sigma[(\chi_M T)_{exp.}-(\chi_M T)_{calcd.}]^2/\Sigma(\chi_M T)_{exp})^2$} and $J = +1.9$ cm^{-1}, $D = 4.1$ cm^{-1}, $g = 2.17$ for **2** ($R = 5.6x10^{-5}$). The values obtained for the magnetic coupling constants and D_{Ni} values are in the range of values reported for other dinuclear Ni^{2+} complexes with *m*-phenylene linkers.[2-4,6] When D_{Ni} was fixed to zero the best fit led to the slightly different set of magnetic parameters: $J = +1.6$ cm^{-1}, $g = 2.16$ and $zJ' = -0.06$ cm^{-1} for **1** ($R = 8.5x10^{-5}$) and $J = +1.5$ cm^{-1}, $g = 2.17$ and $zJ' = -0.06$ cm^{-1} for **2** ($R = 6.0x10^{-5}$). As usual, the extracted J value when $zJ' = 0$ is higher than that extracted for $D = 0$. It should be noted that the D_{Ni} values obtained with $zJ' = 0$ and the zJ' values obtained with $D_{Ni} = 0$ can be considered as the limiting values for these parameters as zJ' and D_{Ni} are strongly correlated and provoke the same result at low temperature. Therefore, these parameters cannot be accurately determined by the fit of the magnetic data, and will require spectroscopic examination. Hereafter, for all the compounds we will keep the data extracted with zJ' fixed to zero for discussions and comparative purposes.

Theoretical DFT studies on **1** confirm that the origin of the ferromagnetic coupling is the spin polarisation mechanism. The magnetic coupling constant calculated from these studies, $J_{DFT} = +4.00$ cm^{-1}, is similar to the experimental value of **1**. Theoretical calculations performed on the recently reported complex $K_2[Ni_2(bpzcb)_3]\cdot 3MeOH\cdot 3H_2O$,[6] which is similar to **2**, but including K^+ ions in their surroundings, afforded $J_{DFT} = +3.9$ cm^{-1}, and also concluded that the ferromagnetic coupling is mediated *via* a spin polarisation mechanism leading to alternating atomic spin densities along the exchange pathway.

The magnetic properties of **3** and **4** were measured in the 2−300 K. range using a magnetic field of 0.1 T and are given in Figure 10. At room temperature $\chi_M T$ is equal to 0.92 cm^3 K mol^{-1} for **3** and 0.91 cm^3 K mol^{-1} for **4**, values close to that expected for two magnetically isolated Cu^{2+} ions with g of 2.18 (**3**) and 2.19 (**4**). Upon cooling, $\chi_M T$ continuously increases and reaches a maximum of 1.02 cm^3 K mol^{-1} at 25 K for **3** and 0.95 cm^3 K mol^{-1} at 12 K for **4**, indicating a relatively weak ferromagnetic coupling between the Cu^{2+} ions through the bpcb and bpzbc ligands. Below this temperature, $\chi_M T$ drops quickly indicating the existence of intermolecular antiferromagnetic interactions between the dinuclear entities and/or ZFS of the triplet ground state. However, given the latter is likely to be very small (of the order 0.001 cm^{-1}), it would appear the former have significant impact on the low temperature magnetic behaviour. This is consistent with the extended structure in **3** and **4** which showed the presence of

multiple H-bonding interactions (Figure S2).

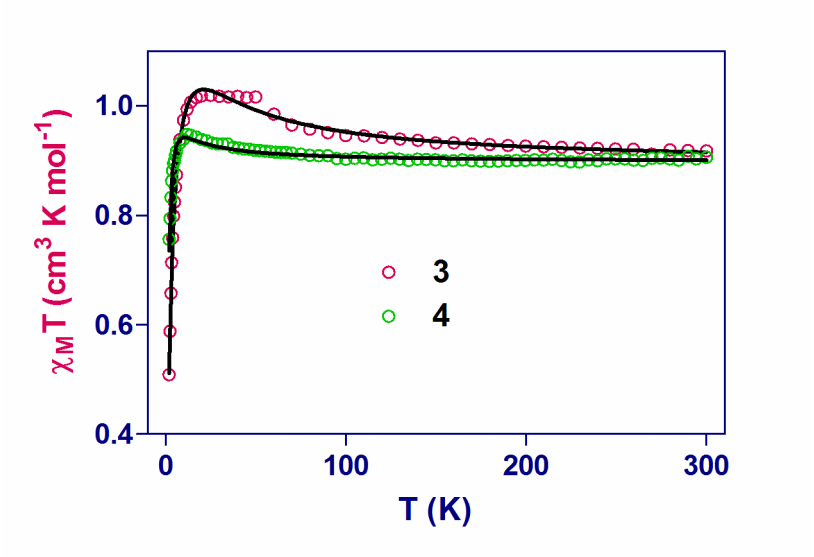

Figure 10: Temperature dependence of the $\chi_M T$ product for complexes **3** and **4**.

The susceptibility data of **3** and **4** were analysed using the following Hamiltonian:

$$\hat{H} = -J\hat{\boldsymbol{S}}_1\hat{\boldsymbol{S}}_2 + \beta(g_1\boldsymbol{S}_1 + g_2\boldsymbol{S}_2)H - zJ'\langle S_z\rangle\boldsymbol{S}_z \quad \text{eq. 2}$$

where the second term corresponds to the Zeeman perturbation and the last term describes the intermolecular interactions using the mean-field approach. The best fit of the experimental magnetic susceptibility data with the above Hamiltonian afforded the following parameters: J = +26.6 cm^{-1}, g = 2.18 and zJ' = −0.51 cm^{-1} for **3** (R = 1.2 x 10^{-4}) and J = +5.7 cm^{-1}, g = 2.19 and zJ' = −0.27 for **4** (R = 2.6 x 10^{-5}). The value of the magnetic coupling constant for **3** is similar to that obtained for the compound [Cu$_2$(mbpb)$_2$] previously reported by us,[3] and larger than other values found for related compounds that present ferromagnetic coupling due to a spin polarisation mechanism.[2,4]

DFT calculations confirm that the magnetic coupling is due to a spin polarisation mechanism with J_{DFT} = +21.5 cm^{-1}, which agrees rather well with the experimental value. In order to know the effect of having an additional nitrogen atom in the bridging pathway, the pyrimidine rings were substituted by pyridine rings. For this model, J_{DFT} = +20.6 cm^{-1}, suggesting that this substitution has no significant influence on the magnitude of J_{DFT}. Although the DFT calculated value J_{DFT} = +12.6 cm^{-1} for **4** is higher than the experimental one (which could be due to inherent limitations of the method), it clearly indicates that the ferromagnetic interaction found for **4** is weaker than those observed for **3** (as observed experimentally in Figure 10), and the closely related complex [Cu$_2$(mbpb)$_2$(CH$_3$CN)$_2$] (J_{DFT} = +25.3 cm^{-1}),[3b] despite the fact that all of these species possess five coordinate Cu^{2+} ions with only small differences in coordination geometries. The lowest shape measures correspond to square pyramid (SPY-5), trigonal bipyramid (TBPY-5) and vacant octahedron (vOC-5) with values of 3.04, 3.64 and 3.72 for **3**, 2.95, 3.76 and 3.12 for **4** and 2.28, 5.07 and 2.64 for [Cu$_2$(mbpb)$_2$(CH$_3$CN)$_2$].[3b] The spin density map for the triplet ground state of the Cu$_2$ unit (the map for complex **4** is given as an example in Figure 11) clearly confirms that that the magnetic coupling takes place through a spin polarisation mechanism, as the π pathway of the

organic skeleton displays an alternating sign of the spin densities.

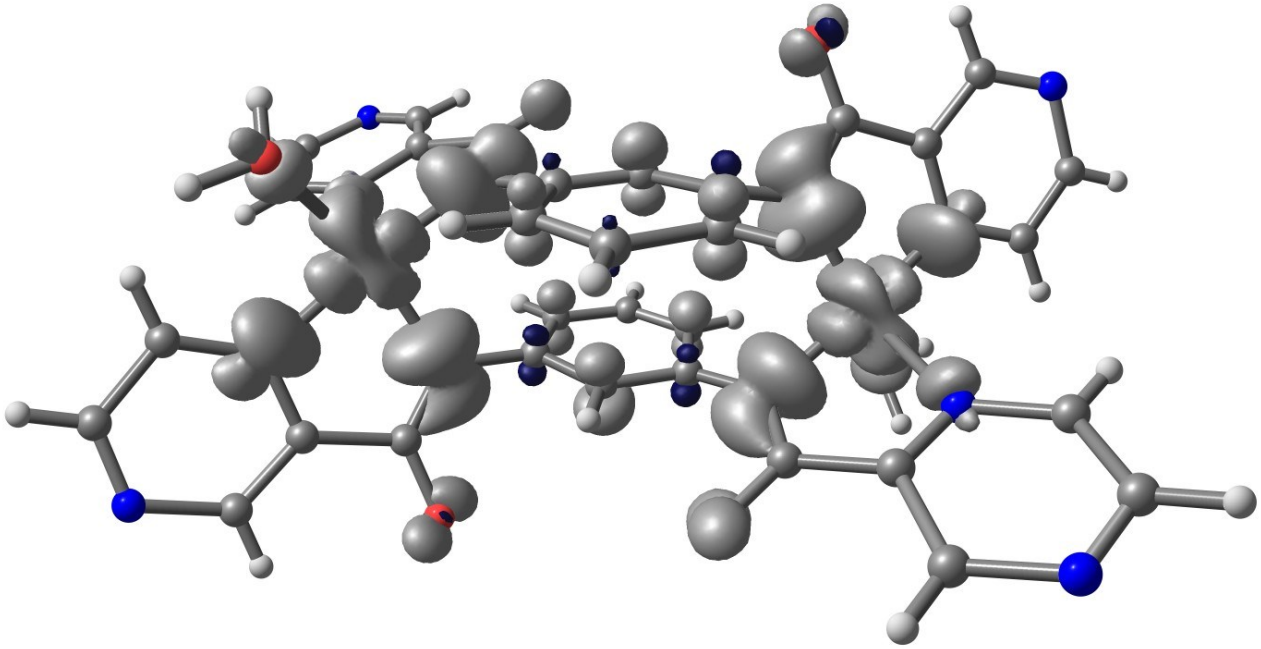

Figure 11. Calculated spin density distribution for the ground triplet spin configuration of **4**. Grey and blue contours represent positive and negative spin densities respectively (cut-off at 0.002 $e \cdot Bohr^{-3}$).

It is worth noting that DFT calculations carried out on a model compound built from **4** by replacing the pyrazine rings for pyrimidine rings indicates that this replacement does not significantly modify the magnetic exchange interaction between the Cu^{2+} ions. Therefore, it is reasonable to conclude that neither the small differences in the Cu^{2+} coordination sphere nor the disposition of the nitrogen atoms of the aromatic rings joined to the *m*-phenylene bridged through the amidate group (*meta* for pyrimidine and *para* for pyrazine), are at the origin of the significant differences between the *J* value for **4** and those found for closely related complexes. In view of this, the origin of such a considerable difference should be found in the geometry adopted by the mpbp, bpcb and bpzcb bridging ligands. At a glance, one can realise that the planes of the amidate groups on both sides of the *m*-phenylenediamine central ring are not coplanar, but rather form different dihedral angles with this latter ring. Moreover, the difference between these dihedral angles (T_2 and T_1) is larger for **4** (46.58°) than for **3** (33.87°) and other related dinuclear complexes, such as $[Cu_2(mbpb)_2(CH_3CN)_2]$[3b] (27.64°) and $[Cu_2(mbpb)_2]$[3a] (5.82°). Interestingly, there exists a linear correlation between this difference, namely T_2-T_1, and the calculated J_{DFT} values (see Figure 12), so that the ferromagnetic interactions increases as T_2-T_1 is smaller. This fact can be correlated to the loss in effectiveness of the spin polarisation mechanism as T_2-T_1 increases (see Figure 12).

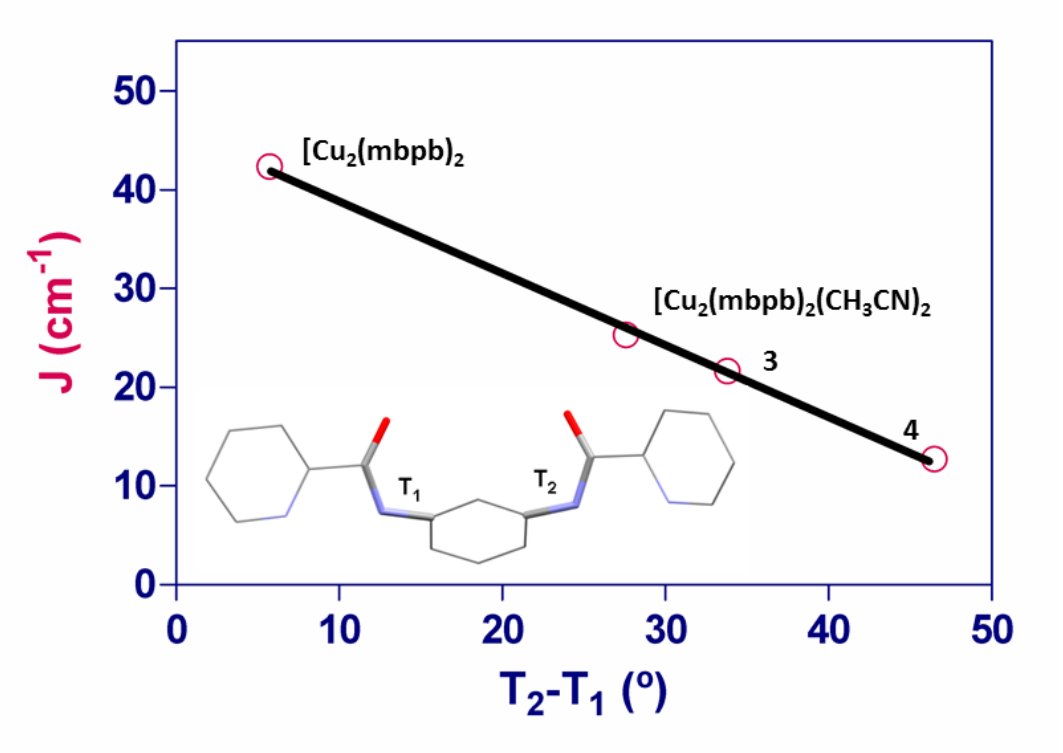

Figure 12: Linear correlation between the calculated *J* values and the T_2-T_1 difference where T2 and T1 represent the dihedral angles between the amidate planes and the plane of the central *m*-phenylene ring.

The magnetic properties of compound **5** were measured in the 2−300 K. range with a magnetic field of 0.1 T and are shown in Figure 13 in the form of the temperature dependence of $\chi_M T$ product (χ_M being the magnetic susceptibility per Ni_3 unit). At room temperature, the $\chi_M T$ value of 3.33 cm^3 K mol^{-1} is close to that expected for three magnetically isolated Ni^{2+} ions with $S_{Ni} = 1$, $g = 2.09$. Upon cooling, $\chi_M T$ decreases continuously, first slowly until 50 K and then more sharply to reach a value 1.16 cm^3 K mol^{-1} at 2.0 K. This behaviour is consistent with a dominant antiferromagnetic interaction between the metal ions. The field dependence of the magnetisation at 2.0 K (inset Figure 13) shows a slow increase of the magnetisation with field to reach a value of 3 Nβ at 5 T. This value is much lower than the expected saturation value for three ferromagnetically coupled Ni^{2+} ions (6 Nβ), which suggests the existence of two competing interactions: ferromagnetic exchange between Ni1 and Ni2 (due to the spin polarisation mechanism through the *m*-phenylendiamide moiety (J_1)) and antiferromagnetic exchange (J_2) between Ni2 and Ni3, through the pyrimidine bridging fragment (Figure 14), which should be stronger than J_1.

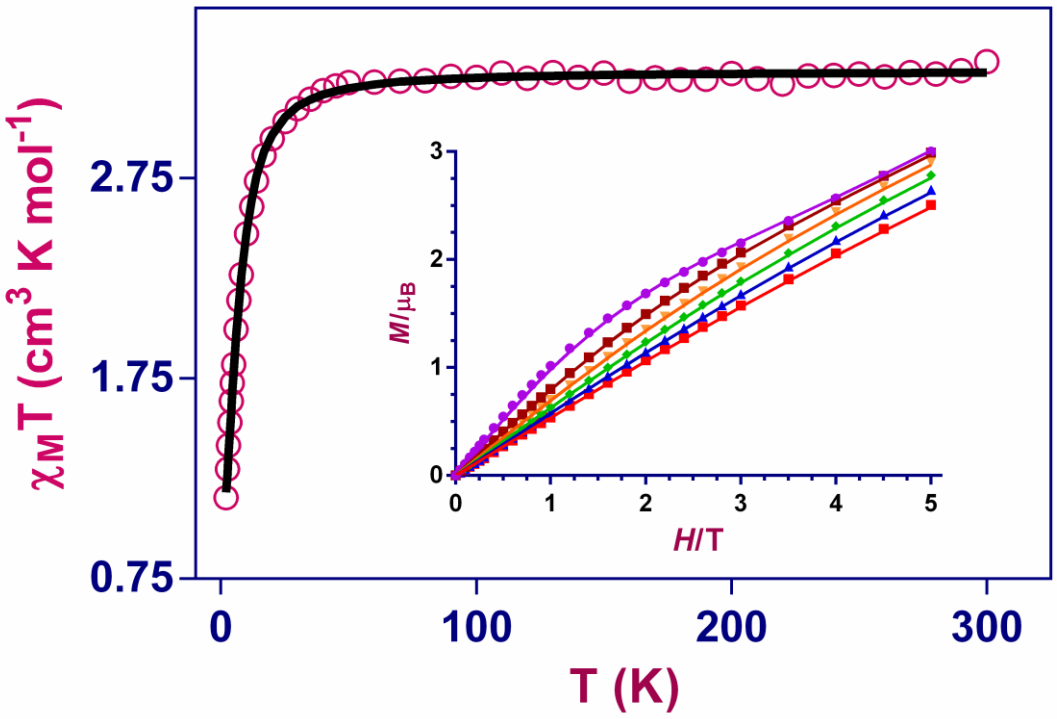

Figure 13: a) Temperature dependence of the $\chi_M T$ product for **5** measured in the 2−300 K. range using a magnetic field of 0.1 T**.** Inset: Field dependence of Magnetisation at different temperatures. Solid lines represent the best fit.

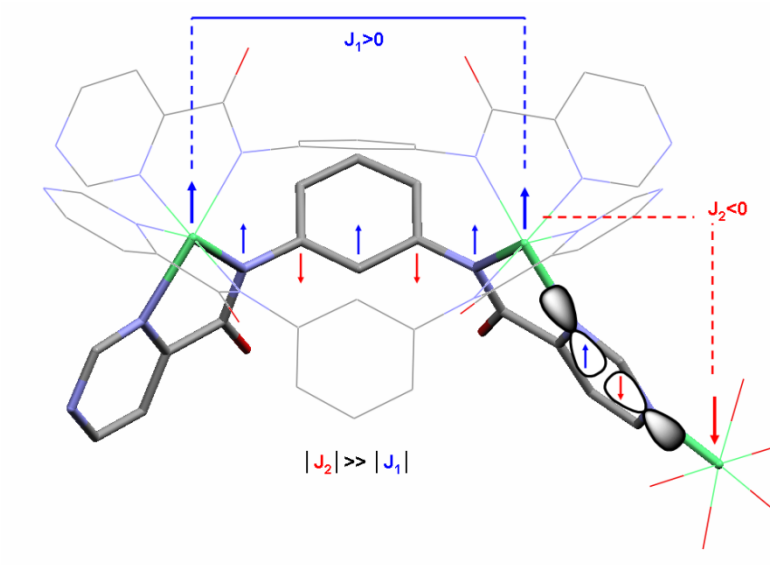

Figure 14: Scheme illustrating the magnetic coupling pathways in complex **5**.

Simulation of the $\chi_M T$ *vs* T curves for different sets of magnetic parameters indicate that the anisotropy of the metal ions is irrelevant compared to J_2, since the plots are virtually identical when $D_{Ni} = 0$ or D_{Ni}

= 4 cm^{-1}, all other parameters being constant. In view of the negligible influence of D_{Ni} on the simulation of the magnetic properties, and to avoid over-parameterisation, the magnetic data were modelled with the following Hamiltonian for a trinuclear Ni^{2+} system with D_{Ni} fixed to zero:

$$\widehat{\boldsymbol{H}} = -J_1\widehat{\boldsymbol{S}}_{Ni1}\widehat{\boldsymbol{S}}_{Ni2} - J_2\widehat{\boldsymbol{S}}_{Ni2}\widehat{\boldsymbol{S}}_{Ni3} + D_{Ni}\left(\widehat{\boldsymbol{S}}^2_{Ni1z} + \widehat{\boldsymbol{S}}^2_{Ni2z} + \widehat{\boldsymbol{S}}^2_{Ni3z}\right) + g\beta H(S_{Ni1} + S_{Ni2} + S_{Ni3}) \quad \text{eq. 3}$$

where J_1 is the magnetic coupling constant between Ni1 and Ni2 through the bpcb ligands belonging to the Ni_2 unit and J_2 represents the magnetic coupling between Ni2 and Ni3 through the pyrimidine ring. Simultaneous fitting of the susceptibility and magnetisation data using the PHI program[14] led to the following parameters: J_1 = +4.4 cm^{-1}, J_2 = −5.6 cm^{-1} and g = 2.09 (R = 7.4x10^{-5}). When the D parameter is allowed to vary freely the same values of the parameters are obtained with D ~0.07 cm^{-1}. The value of J_1 is higher but still close to the value extracted for compound **1**, while J_2 is antiferromagnetic in nature and, as expected, stronger than J_1. The value of J_2 agrees well with those found in literature for pyrimidine bridged polynuclear Ni^{2+} compounds.[15]

Although the structure of complex **6** could not be accurately solved by single crystal X-ray crystallography, we have analysed its magnetic properties since it is isostructural to **5** (Figure 15). The data supports the existence of a ferromagnetic interaction between the Ni^{2+} ions, and an antiferromagnetic interaction between the Co^{2+} and Ni^{2+} ions through the pyrimidine ring, the latter interaction being stronger. At room temperature, the $\chi_M T$ value (4.77 cm^3 K mol^{-1}) is larger than that expected for two Ni^{2+} (S = 1, g = 2) and one Co^{2+} (S = 3/2, g = 2) magnetically isolated ions (3.875 cm^3 K mol^{-1}). This fact is is indicative of an unquenched orbital contribution of the Co^{2+} ion in a distorted octahedral geometry. When the temperature is lowered, the $\chi_M T$ product decreases, first slightly from room temperature to 100 K and then sharply to a value of 1.82 cm^3 K mol^{-1} at 2 K. This decrease is mainly due to the depopulation of the high energy spin-orbit coupled levels of the Co^{2+} ion. The field dependence of the magnetisation at 2 K (inset Figure 15) clearly shows a slow increase of the magnetisation with field without reaching saturation at the maximum applied magnetic field of 5 T. Moreover, the expected saturation value at 5 T and 2 K should be 6 Nβ (previous studies have shown that the contribution of an octahedral Co^{2+} complex to the magnetisation value at 2 K and 5 T is approximately 2 Nβ).[16] However, the observed value of 4.7 Nβ is rather low. This behaviour could be due to the presence of appreciable magnetic anisotropy and possible competing ferromagnetic and antiferromagnetic interactions between the Ni^{2+} ions of the Ni_2 unit, and between Ni^{2+} and Co^{2+} ions through the pyrimidine ring, respectively.

If, for the sake of simplicity, we assume C_{4v} local symmetry for the distorted octahedral $CoNO_5$ coordination polyhedron of **6** (the Co-$N_{pyrimidine}$ bond distance is significantly larger than the Co-O bond distances), the triplet $^4T_{1g}$ ground state for purely O_h symmetry splits into an orbital singlet $^4A_2$ and an orbital doublet ^4E, the energy gap between them being the axial splitting parameter, Δ (positive in this case). The $^4A_2$ and ^4E levels are split in turn by second order spin-orbit coupling leading to two and four Kramers doublets, respectively. When Δ is large enough and positive, only the two lowest Kramers

doublets arising from the $^4A_2$ ground term, Γ_6 and Γ_7, are thermally populated. Then, the energy gap between these two Kramers doublets can be considered as an axial zero-field splitting (ZFS) within the quartet state. In this case, the magnetic properties for the $CoNO_5$ fragment could be interpreted by using the Hamiltonian $\boldsymbol{H} = D[\boldsymbol{S}_z^2 - S(S+1)/3] + E(\boldsymbol{S}_x^2 - \boldsymbol{S}_y^2) + g\mu_B H\boldsymbol{S}$, where S is the spin ground state, D and E are the axial and transverse magnetic anisotropies, respectively, μ_B is the Bohr magneton and H the applied magnetic field. If $E = 0$, then $2D$ represents the energy separation between ±1/2 and ±3/2 doublets arising from second order SOC of the quartet ground state of the distorted octahedral Co^{2+} ion. If $D > 0$ the $M_s = \pm 1/2$ doublet is below the $M_s = \pm 3/2$ doublet and *vice versa*. In view of the above considerations, the magnetic data for **6** were modelled with the following Hamiltonian

$$\widehat{\boldsymbol{H}} = -J_1\widehat{\boldsymbol{S}}_{Ni1}\widehat{\boldsymbol{S}}_{Ni2} - J_2\widehat{\boldsymbol{S}}_{Ni2}\widehat{\boldsymbol{S}}_{Co} + D_{Ni}\left(\widehat{\boldsymbol{S}}_{Ni1z}^2 + \widehat{\boldsymbol{S}}_{Ni2z}^2\right) + D_{Co}[\boldsymbol{S}_z^2 - S(S+1)/3] + g_{Ni}\beta H(S_{Ni1} + S_{Ni2}) + g_{Co}\beta H S_{\mathrm{Co}} \quad \text{eq. 4,}$$

In order to avoid overparametrization, D_{Ni} was fixed to zero and g_{Co}, g_{Ni} were assumed to be equal. The best fit led to the following parameters: $J_1 = +1.8$ cm^{-1}, $J_2 = -2.8$ cm^{-1}, $g = 2.23$ and $D_{Co} = 64.5$ cm^{-1} ($R = 1.5\text{x}10^{-4}$). These results support, as in **5**, the antiferromagnetic interaction between the Ni^{2+} and Co^{2+} ions through the pyrimidine ring. As expected, J_2 describing the CoNi interaction in **6** is weaker than J_2 describing the NiNi interaction in **5**. Moreover, the D_{Co} value is similar to those found for distorted octahedral Co^{2+} mononuclear complexes.[17] Nevertheless, the extracted parameters should be taken with caution due to the crudeness of the model employed.

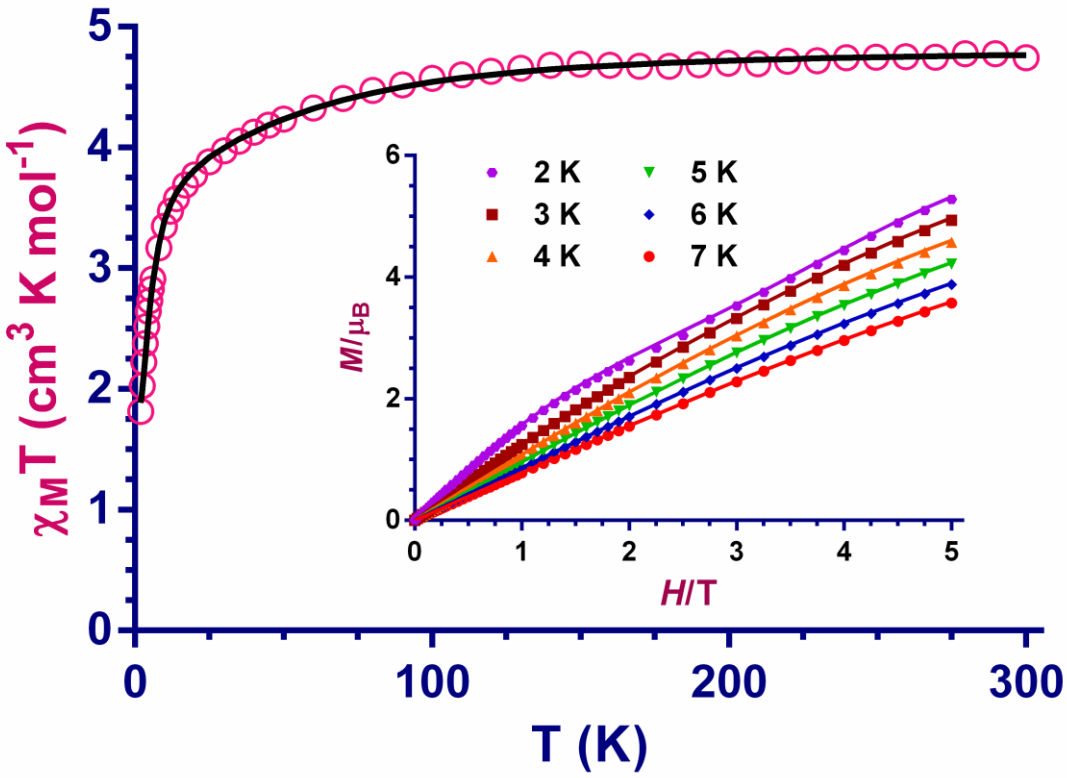

Figure 15: Temperature dependence of the $\chi_M T$ product for **6** measured in the 2−300 K. range with an applied magnetic field of 0.1 T Inset: Field dependence of the magnetisation at different temperatures. Solid lines represent the best fit results.

The temperature dependence of the $\chi_M T$ product of **7** is shown in Figure 16 in the form of the temperature dependence of $\chi_M T$ product (χ_M being the magnetic susceptibility per Ni_4Mn_3 unit). At room temperature, the $\chi_M T$ value (13.47 cm^3 K mol^{-1}) matches well with the expected value for four non-interacting Ni^{2+} ions and three non-interacting Mn^{3+} ions, assuming a *g*-value of 2 (13 cm^3 K mol^{-1}). The value stays roughly constant as the temperature is lowered, and at approximately 130 K the $\chi_M T$ product decreases gradually, first slowly until 25 K and then sharply up to 7.69 cm^3 K mol^{-1} at 2 K, suggesting the presence of predominant antiferromagnetic interactions, in addition to zero-field splitting (ZFS) effects and possible intermolecular interactions between the adjacent complexes. The field dependence of the magnetisation at 2.0 K (Figure S10) shows a slow increase of the magnetisation with the field to reach a value of 12.6 Nβ at 5 T. This curve is below the Brillouin function expected for four Ni^{2+} and three Mn^{3+} ions (saturation value Ms = 20 Nβ), which can be due to the existence of both dominant antiferromagnetic interaction and significant magnetic anisotropy arising from Ni^{2+} and Mn^{3+} ions. To support the existence of a dominant antiferromagnetic interaction between the Ni^{2+} and Mn^{3+} ions in this compound, we have subtracted the contribution of the three Mn^{III}(acen) units (which are known to have a significant ZFS) from the $\chi_M T$ *vs* T plot of **7**, so that only the contribution of the Ni^{2+} ions remains. The resulting curve

(Figure 16) shows a decrease below 75 K to reach a minimum at ~10 K, which confirms the overall antiferromagnetic coupling between Ni^{2+} and Mn^{3+} ions. Below 10 K the ensuing curve increases until 2 K, which could be due to parallel correlation of the non-compensated spins, resulting from the antiferromagnetic interaction between Mn^{3+} and Ni^{2+}, along the plane.

The overall antiferromagnetic interaction in **7** can arise from the competition between the following exchange interactions: (i) ferromagnetic interactions between Ni^{2+} ions belonging to the dimeric unit through the spin polarisation mechanism as for compounds **1**, **5** and **6**, (ii) ferro- or antiferromagnetic interactions between the Ni^{2+} and Mn^{3+} ions through the oxygen atoms of the carboxamide group of the ligands. It is worth mentioning that ferromagnetic and antiferromagnetic interactions have been reported for other Mn^{3+}-Ni^{2+} complexes containing different bridging ligands between these metal ions,[18] and (iii) an antiferromagnetic interaction between the Ni^{2+} and Mn^{3+} ions through the nitrogen atoms belonging to the pyrimidine rings of the ligands, as observed for compounds **5** and **6**.

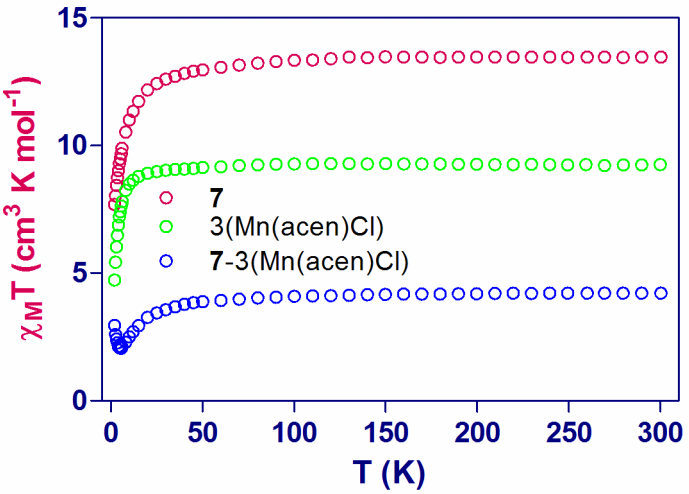

Figure 16: Temperature dependence of the $\chi_M T$ product for **7** (red circles), three units of [Mn(acen)Cl] (green circles) and $\chi_M T$ (**7**)-3$\chi_M T$ (Mn(acen)Cl) (blue circles). The magnetic properties of of [Mn(acen)Cl] were measured from a fresh prepared sample of this compound.

The magnetic properties of the chain compounds **8-10** in the form of $\chi_M T$ *vs* T (χ_M is the magnetic susceptibility per Ni_2Ln unit), are shown in Figure 17.

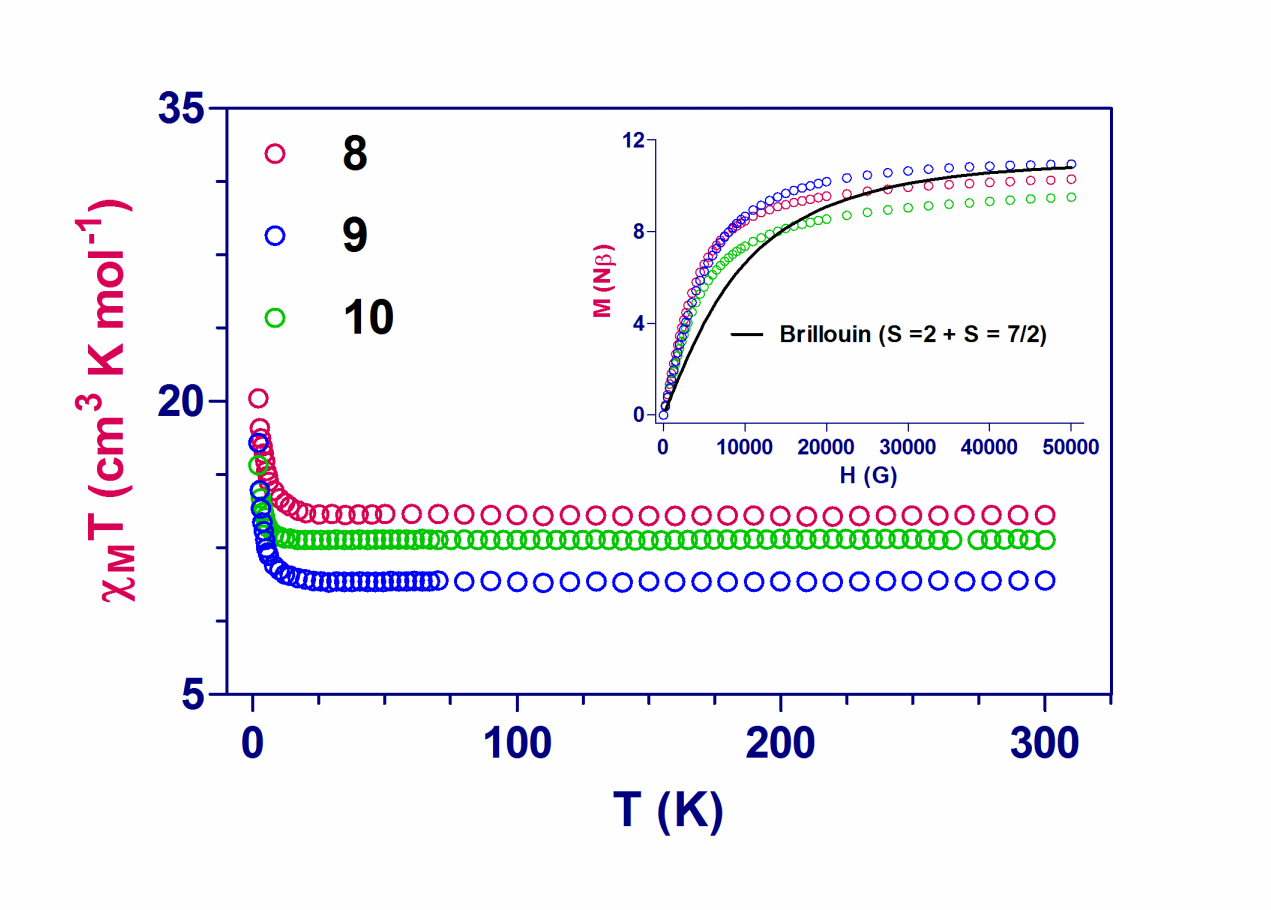

Figure 17: Temperature dependence of the $\chi_M T$ product under an applied magnetic field of 0.1 T in the 2-300 K temperature range and the field dependence of magnetisation, *M*, at 2 K (inset) for **8-10**.

The room-temperature $\chi_M T$ values for **8-10** (Table 2) are close to the value expected for two uncoupled Ni^{2+} ions (S =1, g = 2, $\chi_M T$ = 1 cm^3 K mol^{-1}) and one Ln^{3+} ion. On lowering temperature, the $\chi_M T$ value remains almost constant until approximately 20 K, and below this temperature increases sharply to reach (at 2 K) the values indicated in Table 2. The $\chi_M T$ values at 2 K for **8-10** are somewhat larger than that expected for two ferromagnetically coupled Ni^{2+} ions and one isolated Ln^{3+} ion, confirming the existence of ferromagnetic exchange between the Ni^{2+} and Ln^{3+} ions along the chain.

Table 2.- Direct current magnetic data for the complexes **8-10**.

Compound	Theoretical $\chi_M T_{300K}$ value (cm^{3}Kmol^{-1})[a]	Experimental $\chi_M T_{300K}$ / $\chi_M T_{2K}$ (cm^{3}Kmol^{-1})	Theoretical M_{sat} value (Nβ)[b]	Experimental M_{sat} value (T =2 K, H = 5 T) (Nβ)
8	13.82	14.2 / 20.2	13	10.27
9	9.875	10.8 / 17.9	11	10.93
10	13.82	12.9 / 16.7	13	9.49

[a] $\chi_M T = \frac{N\beta^2}{3k}\{g_J^2 J(J+1)\}$ [b] $M = NJ\mu_B;\ J = L+S\ ;\ g_J = \frac{3}{2} + \frac{S_T(S_T+1) - L(L+1)}{2J(J+1)}$

The temperature dependencies of the $\chi_M T$ products for these compounds do not show the typical decrease due to the depopulation of the m_j sublevels of the Ln^{3+}. This depopulation effect are likelymasked by the ferromagnetic interaction along the chain. For **9** the experimental M vs H plot is above the Brillouin function for two ferromagnetically coupled Ni^{2+} ions and one isolated Gd^{3+} ion, as expected for the existence of ferromagnetic interaction between the Ni^{2+} and Gd^{3+} ions.

The field dependence of the magnetisation for complexes **8** and **10** at $T = 2$ K (Figure 17, inset) shows a rapid increase of the magnetisation at low field to almost reach saturation at a magnetic field of 5 T. However the magnetisation values at this field are lower compared to those calculated (Table 2). This difference is typically due to crystal-field effects leading to significant magnetic anisotropy.[19] In spite of the ferromagnetic interactions along the chain and the magnetic anisotropy of the Tb^{3+} ions, complexes **8** and **10** do not show any out-of-phase signals above 2 K and therefore they do not present either single-chain magnet (SCM) behaviour or single molecule magnet (SMM) behaviour above this temperature.

Conclusions

The use of the ligands 1,3-bis(pyrimidine-2-carboxamide)benzene (H_2bpcb) and 1,3-bis(pyrazine-2-carboxamide)benzene (H_2bpzcb) allows for the formation of dinuclear triple-stranded Ni_2 anionic complexes (**1** and **2**) and dinuclear double-stranded neutral Cu_2 complexes (**3** and **4**). Both types of complexes present ferromagnetic interactions between metal ions through a spin polarisation mechanism, as supported by DFT calculations.

The magnitude of the exchange coupling in **4** is somewhat smaller than that observed for **3** and other previously reported, closely related complexes such as $[Cu_2(mbpb)_2(CH_3CN)_2]$ and $[Cu_2(mbpb)_2]$. DFT calculations show that there exists a linear relationship between the magnitude of the magnetic interaction and T_2-T_1, where T_2 and T_1 represent the dihedral angles between the plane of the *m*-phenylene ring and the plane of each of the carboxamide group, such that the ferromagnetic coupling decreases as T_2-T_1 increases. The origin of this correlation can be found in the fact that the increase of T_2-T_1 decreases the effectiveness of the spin polarisation mechanism and, as a, consequence, the *J* value. Compound **4** has the largest T_2-T_1 value and therefore shows the smallest magnetic exchange coupling value. Interestingly, DFT calculations reveal that the value of the magnetic coupling constant does not significantly change when pyrazine rings in the ligand are replaced by pyrimidine rings.

Following the "complex as ligand" strategy, the dinuclear $[Ni_2(L)_3]^{2-}$ (L = bpcb and bpzcb) units of **1** and **2** can be used as building blocks to be assembled with transition and rare earth metal ions and preformed complexes, affording unusual homo- and heterometallic species, such as (i) unique, neutral, bent trinuclear molecules $[M^{II}Ni^{II}_2(bpcb)_3]\cdot xH_2O$ (M^{2+} = Ni and Co), where the M^{2+} ions are joined to the Ni_2 unit through the nitrogen atom of one of the pyrimidine rings; (ii) chain complexes $[\{[Ni_2(bpzcb)_3]Tb(H_2O)_5\}(CF_3SO_3)\cdot THF\cdot 5H_2O]_n$ and $[\{[Ni_2(bpzcb)_3]Ln(H_2O)_4(NO_3)\}\cdot 2THF\cdot nH_2O]_n$ (Ln^{3+} = Gd and Tb), where the dinuclear Ni_2 unit is joined to two Ln^{3+} ions through one of the amidate oxygen atoms of two different ligands (either bpcb or bpzcb) and (iii) the 2D honeycomb-like complex $(PPh_4)\{[Ni_2(bpcb)_3]_2[Mn(acen)]_3\}$, where each of the two crystallographically independent Ni_2 mesocate

units of the structure are linked to three different $[Mn^{III}(acen)]^+$ units, one of them through one amidate oxygen atom of each ligand and the other one through two amidate oxygen atoms of two ligands and one pyrimidine nitrogen atom. The fact that the outward nitrogen atoms of the pyrazine ring of the bpzcb ligand are not involved in the coordination to other metal ions could be due to the lower basicity of pyrazine compared to pyrimidine rings. All attempts to obtain polynuclear species using compounds **3** and **4** as building blocks to be assembled with metal ions or complexes failed, likely due to their neutral nature and low solubility.

In the trinuclear molecules $[M^{II}Ni^{II}_2(bpcb)_3]\cdot xH_2O$, where the M^{2+} ions are bonded to the external pyrimidine nitrogen atoms, there exists two competing interactions: one ferromagnetic between the Ni^{2+} ions inside the $[Ni_2(bpcb)_3]^{2-}$ dinuclear unit and one antiferromagnetic between one of the Ni^{2+} ions of the dinuclear unit and the M^{2+} ion through the pyrimidine bridging fragment, which is stronger in magnitude. The 2D honeycomb-like complex $(PPh_4)\{[Ni_2(bpcb)_3]_2[Mn(acen)]_3$ shows a dominant antiferromagnetic interaction between the Ni^{2+} and Mn^{2+}. The Ni_2Ln (Ln^{3+} = Gd, Tb) chain complexes show ferromagnetic interactions within the Ni_2 mesocate unit as well as between the Ni^{2+} of the Ni_2 unit and the Ln^{3+} ions. However, none of these ferromagnetic chains show SCM or SMM behaviour.

Acknowledgements

Authors thank the financial support to the Ministerio de Economía y Competitividad (MINECO), Project CTQ2014-56312-P, the Junta de Andalucía (FQM-195 and the Project of excellence P11-FQM-7756), the University of Granada, the CNRS (Centre National de la Recherche Scientifique), the Brest University and the Agence Nationale de la Recherche (ANR project BISTA-MAT: ANR-12-BS07-0030-01), M.A.P thanks MINECO for a *Juan de la Cierva Incorporación* contract.

References:

1.-Some reviews: a) C. Piguet, G. Bernardinelli and G. Hopfgartner, *Chem. Rev.* 1997, **97**, 2005; b) E. C. Constable, *Polynuclear TransitionMetal Helicates,* in *Comprehensive Supramolecular Chemistry*,vol. 9 (Ed.: J.-P. Sauvage), Elsevier, Oxford, 1996, 213; c) M. Albrecht, *Chem. Rev.* 2001, **101**, 3457; d) M. J. Hannon and L. J.Childs, *Supramol. Chem.* 2004, **16**, 7; e) N. K. Al-Rasbi, H. Adams, L. P. Harding and M. D. Ward, *Eur. J. Inorg. Chem.,* 2007, 4770; f) J.-C. G. Bünzli, Chem. Rev., 2010, **110**, 2729; g) C. Piguet, and J.-C. G. Bünzli, *Handbook on the Physics and Chemistry of Rare Earths*, ed. K. A. Gschneidner Jr, J.-C. G. Bünzli, V. K. Pecharsky, Elsevier Science, Amsterdam, 2010, **40**, 301; h) E. Pardo, R. Ruiz-García, J. Cano, X. Ottenwaelder, R. Lescouëzec, Y. Journaux, F. Lloret and M. Julve, *Dalton. Trans.,* 2008, 2780; i) M. Castellano, R. Ruiz-García, J. Cano, J. Ferrando-Soria, E. Pardo, F. R. Fortea-Pérez, S.-E. Stiriba, M. Julve, and F. Lloret, *Acc. Chem. Res*., 2015, **48**, 510; j) M.-C. Dul , E. Pardo, R. Lescouëzec, Y. Journaux, J. Ferrando-Soria, R. Ruiz-García, J. Cano, M. Julve, F. Lloret, D. Cangussu, C. L.M. Pereira, H. O. Stumpff, J. Pasán and C. Ruiz-Pérez, *Coord. Chem. Rev*., 2010, **254**, 2281; k) T. Glaser, *Chem. Commum.* 2010, **47**,116.

2.- a) M-C. Dul, X. Ottenwaelder, E. Pardo, R. Lescouëzec, Y. Journaux, L-M. Chamoreau, R. Ruiz-García, J. Cano, M. Julve and F. Lloret, *Inorg. Chem.,* 2009, **48**, 5244; b) E. Pardo, M-C. Dull, R. Lescouëzec, L-M. Chamoreau, Y. Journaux, J. Pasán, C. Ruiz-Pérez, M. Julve, F. Lloret, R. Ruiz-García and J. Cano, *Dalton. Trans.,* 2010, **39**, 4786; c) M. Castellano, F. R. Fortea-Pérez, A. Bentama, S.-E. Stiriba, M. Julve, F. Lloret, G. De Munno, D. Armentano, Y. Li, R. Ruiz-García and J. Cano, *Inorg. Chem.*, 2013, **52**, 7645; d) E. Pardo, M. C. Dul, R. Lescouëzec, L. M. Chamoreau, Y. Journaux, J. Pasán, C. Ruiz-Pérez, M. Julve, F. Lloret, R. Ruiz-García, and J. Cano, *Dalton Trans*., 2010, **39**, 4786; e) E. Pardo, D. Cangussu, R. Lescouëzec, Y. Journaux, J. Pasán, F. S. Delgado, C. Ruiz-Pérez, R. Ruiz-García, J. Cano, M. Julve and F. Lloret, *Inorg. Chem.*, 2009, **48**, 4661; f) J. Ferrando-Soria E. Pardo R. Ruiz-García J. Cano, F. Lloret M. Julve, Y. Journaux, J. Pasán and C. Ruiz-Pérez, *Chemistry.* 2011, **17**, 2176; g) J Ferrando-Soria, P. Serra-Crespo, M. de Lange, J. Gascon, F. Kapteijn, M. Julve, J. Cano, F. Lloret, J. Pasán, C. Ruiz-Pérez, Y. Journaux and E. Pardo *J. Am. Chem. Soc*., 2012, **134**, 1530; h) J. Ferrando-Soria, T. Grancha, J. Pasán, C. Ruiz-Pérez, L. Cañadillas-Delgado, Y. Journaux, M. Julve, J. Cano, F. Lloret, E. Pardo, *Inorg. Chem.,* 2012, **51**,7019; i) T. Grancha, A. Acosta, J. Cano, J. Ferrando-Soria, B. Seoane, J. Gascon, J. Pasán, D. Armentano and E. Pardo, *Inorg. Chem.,* 2015, **54**, 10834; j) T. Grancha, M. Mon, F. Lloret, J. Ferrando-Soria, Y. Journaux, J. Pasán, and E. Pardo *Inorg. Chem*., 2015, **54**, 8890; k) J. Ferrando-Soria, J. Pasán, C. Ruiz-Pérez, Y. Journaux, M. Julve, F. Lloret, J. Cano and E. Pardo, *Inorg. Chem*., 2011, **50**, 8694.

3.-a) M.-A. Palacios, A. Rodríguez-Diéguez, A. Sironi, J.-M. Herrera, A.-J. Mota, J. Cano and E. Colacio, *Dalton Trans.* 2009, 8538; b**)** M.-A. Palacios, A. Rodríguez-Diéguez, A. Sironi, J.-M. Herrera, A.-J. Mota, V. Moreno, J. Cano and E. Colacio, *New J. Chem.,* 2009, **33**, 1901; c) E. Colacio, M. A. Palacios, A. Rodrıguez-Dieguez, A. J. Mota, J. M. Herrera, D. Choquesillo-Lazarte and R. Clerac, *Inorg. Chem.,* 2010, **49**, 1826.

4.- a) A.-R. Paital, T. Mitra, D. Ray, W.-T. Wong, J. Ribas-Ariño, J.-J. Novoa, J. Ribas and G. Aromí, *Chem. Commun.* 2005, 5172; b) A.-R. Paital, A.-Q. Wu, G.-C. Guo, G. Aromí, J. Ribas-Ariño and D. Ray, *Inorg. Chem.* 2007, **46**, 2947; c) C. Meseguer, S. Titos-Padilla, M. M. Hänninen, R. Navarrete, A. J. Mota, M. Evangelisti, J. Ruiz and E. Colacio, *Inorg. Chem.*, 2014, **53**, 12092.

5.-I. Fernandez, R. Ruiz, J. Faus, M. Julve, F. Lloret, J. Cano, X. Ottenwaelder, Y. Journaux, and M.-C. Muñoz, *Angew. Chem., Int.Ed.*, 2001, **40**, 3039.

6.- J. Ferrando-Soria, O. Fabelo, M. Castellano, J. Cano, S. Fordham and H.-C. Zhou, *Chem. Commum*., 2015, **51**, 13381.

7.- C.-B. Aakeröy, J. Desper, B. Levin and J. Valdés-Martínez, *Inoganica Chimica Acta* 2006, **359**, 1255.

8.- M. Ray, R. Mukherjee, J. F. Richardson and R. M. Buchanan, *J. Chem. Soc., Dalton Trans.* 1993, 2451.

9.- L. J. Boucher and V. W. Day, *Inorg.Chem.,* 1977, **16**, 1360.

10.- G. M. Sheldrick, *SHELXL-97*. A Program for Crystal Structure Refinement; University of Göttingen, Germany, 1997**.**

11.- A. L. Spek, *PLATON-94 (V-101094), A Multipurpose Crystallographic Tool*, University of Utrecht, The Netherlands, 1994.

12.- A. W. Addison, T. N. Rao, J. Reedijk, J. van Rijn and G. C. Verschoor. J. *Chem. Soc., Dalton Trans.,* 1984**,** 1349.

13.- a) S. Alvarez, P. Alemany, D. Casanova, J. Cirera, M. Llunell and D. Avnir, *Coord. Chem. Rev*. 2005, **249**, 1693; b) D. Casanova, M. Llunell, P. Alemany and S. Alvarez, *Chem. Eur. J.* 2005, **11**, 1479.

14.- N. F. Chilton, R. P. Anderson, L. D. Turner, A. Soncini, and K. S. Murray, *J. Comput. Chem.*, 2013, **34**, 1164.

15.- G. Beobide, O. Castillo, A. Luque, U. García-Couceiro, J. P. García-Terán and P. Román, *Dalton Trans.,* 2007, 2669.

16.- F. Lloret, M. Julve, J. Cano, R. Ruiz-García and E. Pardo, *Inorg. Chim. Acta*, 2008, **361**, 3432.

17.- S. Roy, I. Oyarzabal, J. Vallejo, J. Cano, E. Colacio, A. Bauza, A. Frontera, A. M. Kirillov, M. G. Drew and S. Das, *Inorg. Chem.* 2016, **55**, 8502 and references therein.

18.- a) A. Das, K. Gieb, Y. Krupskaya, S. Demeshko, S. Dechert, R. Klingeler, V. Kataev, B. Buchner, P. Muller, and F. Meyer, *J. Am. Chem. Soc.,* 2011, **133**, 3433; b) H. Miyasaka, A. Saitoh, M. Yamashita and R. Clerac, *Dalton Trans.,* 2008**,** 2422; c) T. Weyhermuller, R. Wagner, S. Khanra, and P. Chaudhuri, *Dalton Trans.,* 2005, 2539; d) Y. Sunatsuki, H. Shimada, T. Matsuo, M. Nakamura, F. Kai, N. Matsumoto, and N. Re, *Inorg. Chem.,* 1998, **37**, 5566; e) C. Kalogridis, M. A. Palacios, A. Rodriguez-Dieguez, A. J. Mota, D. Choquesillo-Lazarte, E. K. Brechin, and E. Colacio, *Eur. J. Inorg. Chem.,* 2011, 5225; f) M. Ledezma-Gairaud, L. W. Pineda, G. Aromi, and E. C. Sañudo, *Inorg. Chim. Acta,* 2015,**434**, 215.

19.-a) S. Titos-Padilla, J. Ruiz, J. M. Herrera, E. K. Brechin, W. Wersndorfer, F. Lloret, and E. Colacio, *Inorg.Chem.*, 2013, **52**, 9620; b) S. Upadhyay, S. Kumar Singh, C. Das, R. Mondol, S. K. Langley, K. S. Murray, G. Rajaraman, and M. Shanmugam, *Chem. Commun.,* 2014, **50**, 8838; c) I. Oyarzabal, J. Ruiz, J. M. Seco, M. Evangelisti, A. Camón, E. Ruiz, D. Aravena, and E. Colacio, *Chem. Eur. J.,* 2014, **20**, 14262; d) K. S. Bejoymohandas, A. Dey, S. Biswas, M. L. P. Reddy, R. Morales, E. Ruiz, S. Titos-Padilla, E. Colacio and V. Chandrasekhar, *Chem. Eur. J*., 2015, **21**, 6449.